Biogeosciences Discuss., https://doi.org/10.5194/bg-2018-325
Manuscript under review for journal Biogeosciences
Discussion started: 10 July 2018

Biogeosciences Discussions Open Access EGU

On biotic and abiotic drivers of the microphytobenthos seasonal cycle in a temperate intertidal mudflat: a modelling study

Raphaël Savelli[1], Christine Dupuy[1], Laurent Barillé[2], Astrid Lerouxel[2], Katell Guizien[3], Anne Philippe[1], Pierrick Bocher[1], Pierre Polsenaere[4], and Vincent Le Fouest[1]

[1]Littoral, Environnement et SociétéS (LIENSs), Université de La Rochelle, UMR 7266, CNRS-ULR, 2 rue Olympe de Gouges, 17000 La Rochelle, France
[2]Mer Molécules Santé (MMS) - EA 21 60, Université de Nantes, Laboratoire Mer Molécules Santé, 2 rue de la Houssinière, 44322 Nantes Cedex, France
[3]CNRS-Université Pierre et Marie Curie, UMR 8222 Laboratoire d'Ecogéochimie des Environnements Benthiques, Observatoire Océanologique de Banyuls-sur-Mer, UMR8222, rue du Fontaulé, 66650 Banyuls-sur-Mer, France
[4]IFREMER, Laboratoire Environnement Ressources des Pertuis Charentais (LER/PC), BP7, 17137 L'Houmeau, France

Correspondence to: Raphaël Savelli (raphael.savelli1@univ-lr.fr)

Abstract.

Microphytobenthos (MPB) from intertidal mudflats are key primary producers at the land-ocean interface. MPB can be more productive than phytoplankton and sustain both benthic and pelagic higher trophic levels. The objective of this study is to assess the contribution of light, mud temperature, and gastropod *Peringia ulvae* grazing pressure in shaping the seasonal MPB dynamics on the Brouage mudflat (NW France). We use a physical-biological coupled model applied to the sediment first centimeter for the year 2008. The simulated data compare to observations including time-coincident remotely sensed and *in situ* data. The model suggests a MPB annual cycle characterized by a main spring bloom, a biomass depression in summer, and a moderate fall bloom. In early spring, high simulated photosynthetic rates due to mud surface temperature (MST) values close to the MPB temperature optimum for photosynthesis and to increasing solar irradiance trigger the onset of the MPB spring bloom. After the bloom, high MST values lead to synoptic events when MPB thermo-inhibition (39.5 % of summer) and limitation by *P. ulvae* grazing (8.7 % of summer) superimpose. During these synoptic events, 14 % of the simulated annual MPB primary production is channeled towards the *P. ulvae* secondary production through ingestion. The model suggests that such a combined effect is highly linked to the MPB biomass depression in summer. The model ability to infer on biotic and abiotic mechanisms driving the seasonal MPB dynamics could open the door to a new assessment of the export flux of biogenic matter at the land-ocean interface and, more generally, of the contribution of productive intertidal biofilms to the coastal carbon cycle.

Biogeosciences Discuss., https://doi.org/10.5194/bg-2018-325
Manuscript under review for journal Biogeosciences
Discussion started: 10 July 2018

1 Introduction

Coastal and nearshore waters receive large amounts of organic matter and inorganic nutrients from land that support a high biological productivity (Mann, 1982; Admiraal, 1984; Hopkinson and Smith, 2005). However, the high turbidity of estuarine influenced coastal waters limits the penetration of downward solar irradiance in the water column and, as such, phytoplankton production (Cloern, 1987; Struski and Bacher, 2006). In subtitdal and intertidal zones, primary production (PP) sustained by benthic microalgae, or microphytobenthos (MPB), can equal or exceed that of phytoplankton (Underwood and Kromkamp, 1999; Struski and Bacher, 2006). MPB are mostly composed of free motile epipelic diatoms and of epipsammic diatoms that live in close association (attached or free-living) with sediment grains (Round, 1971). Epipelic MPB are associated with fine cohesive intertidal sediments and developp within the top few millimiters (Underwood, 2001). During daytime emersion, they migrate at the sediment surface constituting a dense biofilm of a few hundred micrometers (Herlory et al., 2004). They are fully exposed to solar irradiance at low tide promoting PP that can reach values as high as 1.9 $\mathrm{g\,C\,m^{-2}\,d^{-1}}$ (Underwood and Kromkamp, 1999). During the flood, epipelic MPB move downward within the sediment but can be resuspended into the water column (Demers et al., 1987; de Jonge and van Beusekom, 1992, 1995; Lucas et al., 2001; Orvain et al., 2004; Ubertini et al., 2012). Both epipelic and epipsammic MPB are a key resource for higher trophic levels from benthic fauna to birds on bare mudflats (Herman et al., 2000; Kang et al., 2006; Jardine et al., 2015), but also for pelagic organisms such as zooplankton and planktivorous fishes (Perissinotto et al., 2003; Krumme et al., 2008).

On intertidal mudflats, MPB PP rates are mainly constrained by solar irradiance and temperature (Barranguet et al., 1998). The MPB biofilm faces strong daily and seasonal variations of mud surface temperature (MST) caused by heating through solar irradiance during low tide exposure periods (Harrison and Phizacklea, 1985; Harrison, 1985; Guarini et al., 1997) and develops phenological adaptations. Blanchard and Cariou-Le Gall (1994), Barranguet et al. (1998) and Pniewski et al. (2015) showed a light-related seasonal adjustment of photosynthetic parameters (the photosynthetic capacity P^b_{max} and the light saturation parameter E_k) from Production-Irradiance (P-E) curves fitted on the model of Platt and Jassby (1976). Photo-inhibition was rarely observed in the field since epipelic diatoms can achieve "micro-migrations", i.e. a negative phototaxic short-term change of position in the sediment (Kromkamp et al., 1998; Perkins et al., 2001; Cartaxana et al., 2011). With respect to mud temperature, Blanchard et al. (1996) related mathematically P^b_{max} to temperature. Using this relationship, Blanchard et al. (1997) showed that P^b_{max} varies according to seasons suggesting a thermo-inhibition process in response to high mud temperature (> 25 °C). de Jonge (1980) also showed seasonal variations of the carbon (C) to chlorophyll *a* (Chl *a*) ratio, which is a proxy of the physiological state of autotrophic cells, as a function of air temperature (de Jonge et al., 2012). Regarding nutrients, their limiting role on the MPB growth and photosynthetic rate is not evidenced in fine cohesive sediments naturally enriched both from within the sediment and the water column (Underwood, 2001; Cadée and Hegeman, 1974; Admiraal, 1984). Vieira et al. (2016) suggested a likely *in vitro* limitation by dissolved inorganic carbon within biofilms. Benthic diatoms were shown to store ammonium and phosphate within the intracellular matrix (García-Robledo et al., 2010; Yamaguchi et al., 2015) potentially usable for assimilation and growth (Garcia-Robledo et al., 2016). The nutrient limitation of MPB is still in debate.

Biogeosciences Discuss., https://doi.org/10.5194/bg-2018-325
Manuscript under review for journal Biogeosciences
Discussion started: 10 July 2018

At temperate latitudes, the seasonal cycle of MPB is shaped by the prevailing environmental conditions. Seasonal blooms are reported to occur throughout the year, i.e. in spring (De Jong and de Jonge, 1995; Sahan et al., 2007; Brito et al., 2013), summer (Cadée and Hegeman, 1977) and fall (Hubas et al., 2006; Garcia-Robledo et al., 2016). Along the French Atlantic coast, the spring bloom and summer depression observed in the Brouage mudflat in the Marennes-Oléron Bay are explained by optimal temperature conditions and thermo-inhibition, respectively (Blanchard et al., 1997). Reported differences in the observed MPB seasonal cycles are also attributed to the diatom assemblage (Underwood, 1994). In terms of biomass, epipelic diatoms associated with muddy sediments show a higher seasonality caused by a marked exposure to stressful environmental conditions (e.g. cycle of deposition/erosion, dessication, grazing) than less motile epipsammic species buried in coarser sandy sediments (Underwood, 1994). In summer, thermo-inhibition and a high grazing pressure by deposit feeders are suggested to dampen the MPB biomass (Cadée and Hegeman, 1974; Cariou-Le Gall and Blanchard, 1995; Sahan et al., 2007). On intertidal mudflats, the prosobranch gastropod *Peringia ulvae* can reach densities up to 30 000 $\mathrm{snails\,m^{-2}}$ (Sauriau et al., 1989) with a reported maximal ingestion rate of 385 $\mathrm{ng\,chl\,}a\,\mathrm{snail^{-1}\,h^{-1}}$ (Coelho et al., 2011). Such grazing activity may translate into a theoretical uptake of 12 $\mathrm{g\,C\,m^{-2}\,d^{-1}}$ for a C:Chl *a* ratio of 45 $\mathrm{g\,C\,g\,chl\,}a^{-1}$ (Guarini, 1998), which is 6-fold more than the daily maximum MPB PP rate reported for MPB (Underwood and Kromkamp, 1999).

In light of the current knowledge, the role of the abiotic and biotic factors involved in the MPB seasonal dynamics is still unclear. This impedes any future assessment on how global change might impact the MPB dynamics and carbon cycle in the land-ocean continuum. The goal of this study is to quantify the relative contribution of light, temperature and grazing on the MPB seasonal cycle and production on an intertidal mudflat (Marennes-Oléron Bay) of the French Atlantic coast. For this purpose, we use a two-layer physical-biological model representing the MPB and *P. ulvae* compartments to assess the contribution of the three drivers over an annual cycle. In the paper, we describe first the physical-biological coupled model and the *in situ* and remotely sensed data used to investigate the MPB seasonal cycle. Second, we assess the relative contribution of light, MST and *P. ulvae* grazing on the MPB dynamics and PP, and we analyze the model sensitivity to key biological constants. Finally, we discuss the role of light, temperature and grazing in the MPB seasonal cycle and the future challenges of modelling the MPB contribution to the carbon cycle at the land-ocean continuum.

2 Material and methods

The study area is the Pertuis Charentais sea on the French Atlantic coast. It is a shallow semi-enclosed sea characterized by semi-diurnal tides and a macrotidal regime. The tidal range is $\sim$ 6 m during spring tides. The intertidal zone has two main mudflats composed of fine cohesive sediments, i.e. the Brouage mudflat (42 $\mathrm{km^2}$) and the Aiguillon mudflat (28.7 $\mathrm{km^2}$) (Fig. 1). The study site (45°54'50"N, 01°05'25"W) is located on the Brouage mudflat (Fig. 1). It is composed of fine cohesive sediments (median grain size of 17 µm and 85 % of grain with a diameter lower than 63 µm; Bocher et al., 2007) and sheltered from Atlantic swells by the Ile d'Oléron (Pascal et al., 2009).

Biogeosciences Discuss., https://doi.org/10.5194/bg-2018-325
Manuscript under review for journal Biogeosciences
Discussion started: 10 July 2018

2.1 Observations

A large multiparametric dataset of physical and biological measurements collected in the Pertuis Charentais was used to constrain the model run and to compare with the model outputs. We provide here a summary of the data used along with their respective references, where a detailed methodology of each measurements can be found.

2.1.1 *In situ* data

Atmospheric and hydrologic forcings were required to set the temperature and light environment that constrained the physical/biological model. Atmospheric forcings (Fig. 3a-e) consisted in meteorological observations (shortwave radiation, air temperature in the shade, atmospheric pressure above the sea, wind speed and relative humidity) acquired at the Meteo France weather station located near the airport of La Rochelle (46°10'36"N, 1°11'3"W; data available online: https://publitheque.meteo.fr; Fig. 1). Hydrology was represented by the absence or presence of seawater at the study site of the Brouage mudflat. Emersion/immersion periods were determined by the observed water height at the tide gauge of La Rochelle-La Pallice (46°9'30"N, 1°13'14"W, data Service Hydrographique et Océanographique de la Marine (SHOM) / Grand Port Maritime La Rochelle-La Pallice; data available online: http://data.shom.fr/) corrected by the bathymetry at the study site. The bathymetry (3.204 m above chart datum) was extracted from a digital elevation model (Litto3D® 2010 Charente Maritime by the Institut National de l'Information Géographique et Forestière (IGN) and the SHOM) at pixels corresponding to the study site (Fig. 1). The weather and tide gauge stations were located $\sim$ 30 km away from the study site. Atmospheric and hydrologic forcings were one hour frequency from January 1, 2008 (00:00 AM) to December 31, 2008 (11:00 PM). They were linearly interpolated at the time step of the model (6 min).

In order to validate the model, we used daily measurements of MST (1^{st} cm), Chl *a* concentration (1^{st} cm) and *Peringia ulvae* biomass and density from a multiparametric dataset collected in February 16 - 24 and July 13 - 26, 2008 at the study site where the model was run (45°54'50"N, 01°05'25"W, Fig. 1). The sampling protocol is fully detailed in Orvain et al. (2014). Monthly data of *P. ulvae* abundance and biomass sampled monthly from April, 2014 to July, 2015 over the Aiguillon mudflat were used to estimate a monthly mean individual weight. The monthly mean individual weight was used to convert the simulated biomass per unit of surface into density per unit of surface. The sampling protocol is given in Bocher et al. (2007). We averaged spatially the *P. ulvae* abundance and biomass data to obtain a monthly mean value for the entire mudflat. Ash-free dry mass (AFDM) was converted to carbon using the relationship derived from Jansson and Wulff (1977) and Remmert (2013) and used by Asmus (1994) for benthic deposit feeders (1 g AFDM = 0.58 $\mathrm{g\,C}$). When the individual weight was not available, the individual height was used to estimate the AFDM (mg) using the formulation of Santos et al. (2005):

$$AFDM = 0.0154H^{2.61}, \quad (1)$$

where H is the total individual height (mm).

Biogeosciences Discuss., https://doi.org/10.5194/bg-2018-325
Manuscript under review for journal Biogeosciences
Discussion started: 10 July 2018

2.1.2 Remote sensing data

Moderate Resolution Imaging Spectroradiometer (MODIS) images from the Terra satellite were downloaded from the USGS Earth Resources Observation and Science Center (http://earthexplorer.usgs.gov/). The Terra MODIS Surface Reflectance Daily L2G Global 250m SIN Grid product (MOD09GQ) contains 250-m surface reflectance in a red band (620-670 nm, band center at 645 nm) and a near-infrared band (841-876 nm, band center at 859 nm). Terra data were used because the morning-pass (10-11h Universal Time) is better adapted than Aqua MODIS data to observe spring low tides at our study site. The data were corrected of atmospheric effects (aerosol, water vapor) and each image was checked for clouds/cirrus and cloud shadows. Cloud-free low-tide scenes were selected to apply a vegetation index. Images were reprojected to UTM/WGS84 coordinate system. The Normalized Difference Vegetation Index (NDVI; Tucker, 1979) was calculated with the reflectance (ρ) in the red (R) and near-infrared (NIR) bands :

$$\mathrm{NDVI} = \frac{\rho(\mathrm{NIR}) - \rho(\mathrm{R})}{\rho(\mathrm{NIR}) + \rho(\mathrm{R})} \tag{2}$$

The NDVI thresholds proposed by Méléder et al. (2003) to identify MPB with SPOT images was adapted for MODIS data and a range of 0 to 0.35 was used in this study. Negative NDVI values were associated with water and null values to bare sediment, while values higher than 0.35 corresponded to macrophytes (macroalgae and seagrass). For the present study, a NDVI time-series was extracted for 2008 (47 scene images) at pixels corresponding to the study site (Fig. 1). Scene images were processed with the ENVI® software.

2.2 The coupled physical-biological model

The coupled model consisted in a mud temperature model coupled to a 3-compartment biological model. The mud temperature model was a thermodynamic model developed by Guarini et al. (1997) resolving heat fluxes at the surface in a 1-cm thick sediment layer. Equations are given in Appendix A and Table A1. It was calibrated and validated on the Brouage mudflat by Guarini et al. (1997). During emersion periods, the simulated MST resulted from heat exchanges between the sun, the atmosphere, the sediment surface, from the conduction between mud and air and from evaporation (Fig. 2). Thermal conduction between mud and seawater was the only heat exchange during immersion periods (Fig. 2). The seawater temperature was simulated according to heat fluxes resulting from thermal conduction between air and seawater, from upward seawater radiation, and from downward solar and atmospheric radiation. The simulated mud temperature was considered homogeneous at the horizontal scale. The heat fluxes were determined according equations given in Table A1 (Appendix A). The MST differential equation (Eq. A1 in Appendix A) was solved with an Euler Cauchy algorithm at a 30-sec time step.

The mud temperature model constrained a 3-compartment biological model, which was modified from Guarini (1998) and Guarini et al. (2000). It is fully detailed in Appendix B. MPB was represented by two compartments including the Chl *a* concentration in the 1$^{\mathrm{st}}$ cm sediment (F, $\mathrm{mg\,chl\,a\,m^{-2}}$) and the Chl *a* concentration within the surface biofilm (S, $\mathrm{mg\,chl\,a\,m^{-2}}$). The variable $S*$ represents the S compartment that incorporated the S instantaneous production of biomass ($\mathrm{mg\,chl\,a\,m^{-2}}$). The model assumed no sediment erosion nor deposition and no horizontal movement of MPB within the sediment. It included

Biogeosciences Discuss., https://doi.org/10.5194/bg-2018-325
Manuscript under review for journal Biogeosciences
Discussion started: 10 July 2018

a scheme of MPB vertical migration between the S and F compartments (Guarini, 1998; Guarini et al., 2000). The migration scheme is summarized in Table 1. The MPB growth rate was constrained by the photosynthetically active radiation (PAR) intensity, the simulated MST, and the grazing pressure. The grazing pressure was represented through a new scalar, Z, representing the *P. ulvae* biomass ($\mathrm{mg\,C\,m^{-2}}$). *P. ulvae* is a very abundant MPB grazer on the Pertuis Charentais intertidal mudflats (Sauriau et al., 1989). The *P. ulvae* growth rate was constrained by the simulated MPB biomass and the MST. The fourth-order Runge-Kutta method was used to solve the biological differential equations with a 6-min time step.

The coupled physical-biological model was run at the study site (Fig. 1) from 1 January to 30 December, 2008. Initial conditions were 100 $\mathrm{mg\,chl}\,a\,\mathrm{m^{-2}}$ for F and 1000 $\mathrm{mg\,C\,m^{-2}}$ for Z. No biomass was set for S at the beginning of the simulation as it started at midnight (i.e. no light). The initial MST was initialised at the seawater temperature (see Eq. A5-8 in Appendix A) at the first period of immersion. A 2008 10-year spin-up was performed before the analysis of the model outputs. The spin-ups and initial biomass conditions allowed for the convergence towards similar values of biomass at the end of each run.

We performed a sensitivity analysis to quantify how all-at-a-time variations in key biological parameters would impact the simulated MPB PP. A Monte-Carlo fixed sampling method (Hammersley and Handscomb, 1964) was used to randomly select values of T_{opt}, T_{max}, T_{optZ}, α_Z, E_k and K_E within observed ranges (Table 3). A total of 10,000 model runs was performed with the same previous initial conditions. Statistical metrics on simulated annual PP according to parameters values and variations (Pearson's correlation coefficient and parameters average, normalized standard deviation, minimum and maximum) were computed.

3 Results

3.1 Mud surface temperature

The simulated temperature of surface mud followed the seasonal cycle of air temperature (Fig. 3d and Fig. 4). During winter-spring (November to April), the simulated mud temperature was 8.6 $\pm$ 3.6 °C in average. The simulated mean temperature was twice in summer-fall (May to October) reaching 16.9 $\pm$ 3.9 °C. The seasonal amplitude of the simulated mud temperature was higher in summer-fall (27 °C) than in winter-spring (18.8 °C). At the synoptic scale, the model reasonably simulated the high frequency (1 min) variations of MST measured at the study site in February and July 2008 (Fig. 4).

3.2 MPB dynamics

In 2008, $S*$ reached a maximum value of 31 $\mathrm{mg\,chl}\,a\,\mathrm{m^{-2}}$ on February 24. The daily maximum values of $S*$ biomass simulated by the model for 2008 were subsampled to match the 2008 NDVI time series data (Fig. 5). Three distinct seasonal phases were identified in both time series using the amplitude of sign change of the $S*$ and NDVI second order time derivatives (Fig. 5). The phase 1 corresponded to the spring bloom during which the biomass in the biofilm and the NDVI data reached their seasonal maximum value (day 1 to 144 and day 1 to 165 in the NDVI and model data, respectively). The phase 2 coincided

Biogeosciences Discuss., https://doi.org/10.5194/bg-2018-325
Manuscript under review for journal Biogeosciences
Discussion started: 10 July 2018

with a summer depression in the simulated MPB biomass and NDVI data (day 145 to 270 and day 166 to 256 in the NDVI and model data, respectively). Finally, the phase 3 showed an increase of both the simulated biomass and NDVI values suggesting a fall bloom (day 271 to 366 and day 257 to 366 in the NDVI and model data, respectively). With respect to the NDVI data, the model showed a 21 days and 14 days longer spring and fall bloom, respectively, and a 35 days shorter summer depression (Fig. 5). Overall, the seasonal cycle of the simulated MPB biofilm compared to that depicted by the remotely sensed NDVI data.

At the seasonal scale, the total MPB biomass ($S + F$) simulated by the model within the 1st cm sediment was the lowest in January and August ($\sim$ 30 $\mathrm{mg\,chl\,}a\,\mathrm{m}^{-2}$) and reached a seasonal maximum in April ($\sim$ 238 $\mathrm{mg\,chl\,}a\,\mathrm{m}^{-2}$, Fig. 6a). The seasonal cycle of the MPB biomass was related to the simulated mean time spent by a MPB cell at the sediment surface (τ_s; Fig. 6ab). During daytime emersion time, a MPB cell spent approximatively 54 minutes in January and August and 12 minutes in April at the sediment surface because of the inverse relationship between total MPB biomass and τ_s (Eq. B5 in Appendix B1). The model reproduced the fortnightly tidal cycle with maximum values of MPB biomass simulated in spring tides (Fig. 6a). The simulated values of biomass of MPB were compared to 2008 time coincident observations (Fig. 6a). In February 2008, the simulated biomass was about 137 $\pm$ 16.3 $\mathrm{mg\,chl\,}a\,\mathrm{m}^{-2}$, which was close but significantly higher compared to the measured total MPB biomass (106.5 $\pm$ 11.3 $\mathrm{mg\,chl\,}a\,\mathrm{m}^{-2}$; Mann Whitney test: p-value < 0.05). In July 2008, the model also overestimated (98 $\pm$ 26.4 $\mathrm{mg\,chl\,}a\,\mathrm{m}^{-2}$) the observed (58.6 $\pm$ 10.3 $\mathrm{mg\,chl\,}a\,\mathrm{m}^{-2}$) MPB biomass (Mann Whitney test: p-value < 0.05), more than in February. Overall, the model simulated values that reasonably compared, in average, to matchup measurements gathered.

As for Chl *a*, the simulated daily mass-specific photosynthetic rates were higher in late winter-spring (0.54 $\pm$ 0.1 $\mathrm{mg\,C\,(mg\,chl\,}a)^{-1}\,\mathrm{h}^{-1}$) than in summer (0.41 $\pm$ 0.06 $\mathrm{mg\,C\,(mg\,chl\,}a)^{-1}\,\mathrm{h}^{-1}$) and fall-early winter (0.25 $\pm$ 0.13 $\mathrm{mg\,C\,(mg\,chl\,}a)^{-1}\,\mathrm{h}^{-1}$) (Fig. 6c). The annual mean of the simulated MPB growth rate in the biofilm was 0.24 $\pm$ 0.07 d^{-1} with a range of values between 0.04 d^{-1} and 0.43 d^{-1}. In the model, the MPB growth rate was related to the C:Chl *a* ratio (see Eq. B9 in Appendix B2). The simulated mean C:Chl *a* ratio varied in a range of values between 16 and 75.5 $\mathrm{g\,C\,g\,chl\,}a^{-1}$ (with a mean value of 34.1 $\pm$ 17.2 $\mathrm{g\,C\,g\,chl\,}a^{-1}$ in winter-spring-fall and 42.7 $\pm$ 20 $\mathrm{g\,C\,g\,chl\,}a^{-1}$ in summer). The simulated annual and daily MPB PP rates were 118 $\mathrm{g\,C\,m}^{-2}\,\mathrm{y}^{-1}$ and 320 $\pm$ 219 $\mathrm{mg\,C\,m}^{-2}\,\mathrm{d}^{-1}$, respectively.

3.3 *P. ulvae* dynamics

The MPB biomass simulated by the model was also constrained by the grazing pressure from the gastropod *P. ulvae*. The simulated density and biomass of *P. ulvae* increased in late spring with a first seasonal peak of ingestion in May 2 (Fig. 7c). The *P. ulvae* density reached a seasonal maximum in August 28 (39 950 $\mathrm{ind\,m}^{-2}$) one months later than the seasonal maximum of *P. ulvae* biomass (July 22, 4.38 $\mathrm{g\,C\,m}^{-2}$, Fig. 7ab). The simulated density and biomass of *P. ulvae* were compared to 2008 time coincident observations (Fig. 7ab). In February, 2008 the simulated density (3308 $\pm$ 8.4 $\mathrm{ind\,m}^{-2}$) was significantly lower than the measured density (5766 $\pm$ 2985 $\mathrm{ind\,m}^{-2}$; Mann Whitney test: p-value < 0.05). In July, 2008 an average density of 11851 $\pm$ 3143 $\mathrm{ind\,m}^{-2}$ was simulated by the model while a significantly higher average density of 17191 $\pm$ 7084 $\mathrm{ind\,m}^{-2}$ was measured (Mann Whitney test: p-value < 0.05). In February, 2008 the simulated biomass of *P. ulvae* was 381.28 $\pm$ 4.5 $\mathrm{mg\,C\,m}^{-2}$, which was significantly lower (Mann Whitney test: p-value < 0.05) than the observed biomass (749.5 $\pm$ 388

Biogeosciences Discuss., https://doi.org/10.5194/bg-2018-325
Manuscript under review for journal Biogeosciences
Discussion started: 10 July 2018

$\mathrm{mg\,C\,m^{-2}}$). In July, 2008 the model underestimated biomass (2809.3 $\pm$ 700.4 $\mathrm{mg\,C\,m^{-2}}$) whereas the measured biomass was 4469.8 $\pm$ 1841.9 $\mathrm{mg\,C\,m^{-2}}$ (Mann Whitney test: p-value < 0.05). The *P. ulvae* gross secondary production simulated by the model was 13.63 $\mathrm{g\,C\,m^{-2}\,y^{-1}}$. Overall, the model reasonably captured the seasonal features depicted by the matchup observations.

3.4 Contribution of light, temperature and grazing to the MPB seasonal cycle

In the model, bottom-up (MST and downward irradiance) and top-down (grazing by *P. ulvae*) processes constrained the simulated MPB growth rate. Light and temperature limitation terms (see Eq. B7 and B8 in Appendix B2) varied between 0 and 1. At each time step, the lowest value was set as the most limiting term constraining the computation of the MPB photosynthetic rate. Over each daytime emersion period, the most limiting bottom-up factor was defined as the factor whose limitation was the longest.

In phase 1, MST and light limited MPB growth 33.3 % and 66.7 % of the time, respectively, because PAR and simulated MST values were lower than the light saturation parameter (E_k, 100 $\mathrm{W\,m^{-2}}$) and the temperature optimum for photosynthesis (T_{opt}, 18 °C), respectively (Table 2).

In phase 2, light was the most limiting factor (60.5%, Table 2), because the daytime duration was the longest over the year (Fig. 8). The increasing daytime duration allowed MPB to grow on two daytime emersion periods at the beginning and at the end of the daytime period. As a result, the simulated MPB growth rate was limited by low light levels over a longer period than during phase 1 and phase 3 (Fig. 8). With respect to temperature, the MPB growth was more limited by MST in phase 2 (39.5 %) than in phase 1 (33.3 % Table 2). The high summer air temperature and solar irradiance heated the mud surface (Fig. 3 and 4), especially when daytime emersion periods occured in the middle of the day (10 AM - 16 PM) in spring tides (Fig. 8) with, as a consequence, simulated MST higher in average than the MPB T_{opt} value (Fig. 9).

In phase 3, the MPB growth rate was limited only by downward irradiance (100 %, Table 2). In fall, solar irradiance on daytime emersion periods decreased faster (slope = - 19.2 $\mathrm{W\,m^{-2}\,d^{-1}}$, p-value < 0.05, corresponding to a deviation from E_k of -19 % $\mathrm{d^{-1}}$) than the MST (slope = -1.34 °C $\mathrm{d^{-1}}$, p-value < 0.05, corresponding to a deviation from T_{opt} of - 7 % $\mathrm{d^{-1}}$).

Figure 9a shows the daily occurence of MPB limitation by the simulated MST over 2008. In phase 1, the simulated MST increased towards T_{opt} and, combined with increasing irradiance, led to a seasonal maximum of the mass-specific photosynthetic rate (Fig. 6c). In early May (phase 1), the mass-specific photosynthetic rate started to decrease due to thermo-inhibition as soon as the MST exceeded T_{opt} (Fig. 6c and 9a), and the MPB biomass remained constant ($\sim$ 200 $\mathrm{mg\,chla\,m^{-2}}$) until the beginning of phase 2 (Fig. 9). In phase 2, the simulated MST was always higher than T_{opt} when temperature limitation occured (Fig. 9a).

With respect to grazing, it was considered limiting for the MPB growth only when the simulated amount of biomass grazed by *P. ulvae* was higher than the simulated MPB biomass produced over the daytime emersion period (Fig. 9b). The top-down control by *P. ulvae* was mostly limiting in phase 2, when the ingested MPB biomass exceeded the MPB PP during 8.7% of the time (Fig. 9b). In phase 2, three high ingestion events were simulated and resulted into peaks of *P. ulvae* density and biomass in June 10, July 23 and August 29 (Fig. 7 and 9b). The simulated MST was higher in average than the temperature

Biogeosciences Discuss., https://doi.org/10.5194/bg-2018-325
Manuscript under review for journal Biogeosciences
Discussion started: 10 July 2018

optimum for grazing (T_{opt_Z}) all days when MPB were grazing-limited and triggered these three high ingestion events (Fig. 9b). The simulated peaks of ingestion rate varied between $\sim$ 180 and 334 $\mathrm{ng\,chl}\,a\,\mathrm{ind}^{-1}\,\mathrm{h}^{-1}$ over 2008 (Fig. 7c). 90 % of the grazing-limited days occured when the MST was already limited the MPB growth rate over 2008 (Fig. 9).

One month after the onset of MPB thermo-inhibition (May 2), a 6-day event of high *P. ulvae* ingestion (> 10 $\mathrm{mg\,C\,d}^{-1}$) starting on June 8 (Fig. 7c) resulted into a sharp decrease of the simulated MPB biomass (Fig. 9b) and coincided with the beginning of phase 2. The MPB biomass grazed by *P. ulvae* during this synoptic event represented 5.35 $\mathrm{g\,C\,m}^{-2}$, which corresponded to a MPB biomass removal of 81 $\mathrm{mg\,chl}\,a\,\mathrm{m}^{-2}$. The combined effect of grazing and thermo-inhibition on the simulated MPB growth lasted 10 days in 2008 (2.7% of the year). It corresponded to a MPB biomass removal representing 14 % of the annual MPB PP (15.8 $\mathrm{g\,C\,m}^{-2}$; Fig. 9).

In the model, the occurrence of temperature or light limitation resulted from the coupling of the fortnightly tidal cycle with the seasonal solar irradiance and air temperature cycles. Over 2008, light was the most limiting factor because of low light levels in fall-winter and the occurrence of early and late daytime emersion periods during neap tides in spring-summer. During summer spring tides, the emersion periods in the middle of the day led to high simulated MST value (> 22 °C), hence limiting the MPB growth rate and promoting the *P. ulvae* grazing activity. The combined effect of thermo-inhibition and grazing in summer resulted into a marked depression of the simulated MPB biomass.

3.5 Annual MPB production sensitivity

A total of 10000 model runs (N) was performed where key biological parameters (T_{opt}, T_{max}, T_{opt_Z}, α_Z, E_k and K_E) were randomly selected within observed ranges (Table 3). The sensitivity analysis resulted in two kinds of model runs according to the sustainability of the MPB PP over the year. Model runs in which PP was sustained (SPP runs, PP > 40 $\mathrm{g\,C\,m}^{-2}\,\mathrm{y}^{-1}$, N = 1817) were distinguished from runs characterized by vanishing PP (VPP runs, PP $\leq$ 40 $\mathrm{g\,C\,m}^{-2}\,\mathrm{y}^{-1}$, N = 8183) according to a graphical representation of the annual PP as a function of the number of runs (Fig. 10).

In SPP runs, the annual production was negatively correlated with the MPB temperature optimum for photosynthesis (T_{opt}, Pearson's R = -0.24, p-value < 0.05) and positively correlated with the MPB temperature maximum (T_{max}, Pearson's R = 0.22, p-value < 0.05; Table 4). The correlation between PP and the MPB temperature amplitude (T_{amp}, the difference between T_{opt} and T_{max}) was even higher than the correlation between PP and T_{opt} and T_{max} (Pearson's R = 0.39, p-value < 0.05; Table 4), suggesting that an increase of T_{amp} (i.e. a decrease of T_{opt} concomittant with an increase of T_{max}) led to an increase of the PP. The mean values T_{amp}, T_{opt} and T_{max} were 15 °C, 19 °C and 34 °C, respectively with relatively low variations of T_{opt} and T_{max} ($\sigma_{norm} \approx 0.14$) in SPP runs (Table 4). In terms of temperature, the use of this set of average values allows a sustainable PP in the model. In VPP runs, the mean value of T_{amp} was 10.1 °C lower than in SPP runs, because the mean T_{opt} value (29 °C) was higher than in SPP runs (19 °C). The maximum value of T_{opt} was 10 °C higher in VPP runs than in SPP runs. The resulting wider range of T_{opt} values led to higher variations in T_{amp} in VPP runs (σ_{norm} = 0.73). However, SPP runs also showed a T_{amp} minimum of 4.5 °C, which is $\sim$ 3-fold lower that the mean amplitude (T_{amp}) value (15 °C). Therefore, in addition to the temperature-related parameters, the light saturation parameter (E_k) played a role in the sustainability of PP over the year.

Biogeosciences Discuss., https://doi.org/10.5194/bg-2018-325
Manuscript under review for journal Biogeosciences
Discussion started: 10 July 2018

While a small positive correlation was evidenced between E_k and PP in VPP runs (Pearson's R = 0.02, p-value < 0.05), E_k was negatively correlated with PP in SPP runs to a larger extent (Pearson's R = -0.56, p-value < 0.05). In SPP runs, the mean value of E_k (77 $\mathrm{W\,m^{-2}}$) was lower than in VPP runs (95 $\mathrm{W\,m^{-2}}$). However, E_k variations were comparable (0.54 < σ_{norm} < 0.64) and the minimum (2.5 $\mathrm{W\,m^{-2}}$) and maximum values (180 $\mathrm{W\,m^{-2}}$) were same in both the SPP and VPP runs. Consequently, annual PP is less sensitive to variations of E_k than to variations of T_{opt} and T_{max}. Nevertheless, in SPP runs, a low value of E_k could sustain PP if T_{amp} was lower than 15 °C. The half-saturation constant for light use (K_E) was not correlated with annual PP in SPP runs (Pearson's R = 0.01, p-value > 0.05). K_E was slightly but negatively correlated with annual PP in VPP runs (Pearson's R = -0.04, p-value < 0.05). In VPP runs, low values of K_E slightly increased the annual PP.

In SPP runs, the temperature optimum for grazing by *P. ulvae* (T_{opt_Z}) showed a low but significant correlation with PP (Pearson's R = 0.16, p-value < 0.05) suggesting that high T_{opt_Z} values resulted in high levels of annual PP. The shape parameter of the temperature grazing function (α_Z) was negatively correlated with PP in SPP runs (Pearson's R = -0.11, p-value < 0.05). However, T_{opt_Z} and α_Z variations were high and of the same extent (σ_{norm} = 0.19 and $\sigma_{norm} \approx 0.6$, respectively) and their mean, maximum and minimum values were very similar in both SPP and VPP runs (Table 4). Overall, the model was therefore sensitive to MPB temperature parameters and to the light saturation parameter. A specific set of these temperature and light related parameters allowed for a sustainable level of MPB production and biomass, which resulted into a significant effect of grazing on the MPB annual production.

4 Discussion

4.1 The MPB seasonal cycle

Our study suggests a MPB seasonal cycle on the Brouage mudflat characterized by three phases in 2008, i.e. a bloom in winter/spring, low biomass levels in summer, and a peak of moderate intensity in fall. Cariou-Le Gall and Blanchard (1995) sampled monthly from March 1992 to February 1993 the MPB Chl *a* concentration within the top 0.5 cm sediment on the Brouage mudflat. Their measurements suggest a bloom in winter/spring and low Chl *a* concentrations in summer, which is consistent with the 2008 NDVI data and MPB biomass simulated by the model. Cariou-Le Gall and Blanchard (1995) did not report any peak of MPB biomass in fall, which may be modulated by the interannual variability driven by the meteorological conditions. In Northern (De Jong and de Jonge, 1995; Sahan et al., 2007) and Southern (Brito et al., 2013) european mudflats, MPB spring blooms are also observed. However, the contribution of underlying abiotic (e.g. air temperature, irradiance, rain, wind) and biotic (e.g. autotrophic species community, predators) factors are likely to be different in shaping the seasonal MPB cycle at such contrasted latitudes.

In the Brouage mudflat, the seasonal cycle of MPB at the sediment surface compares to that depicted by the remotely sensed NDVI data. The simulated MPB biomass in the biofilm and its instantaneous PP are close to maximum values of biomass previously measured in biofilms developping at the surface of very fine sediments of the Brouage mudflat (24 ± 5 $\mathrm{mg\,chl\,}a\,\mathrm{m^{-2}}$; Herlory et al., 2004). Also, the mean time spent by MPB cells at the surface in the model (36.6 ± 12 min) is consistent with the estimate reported by Blanchard et al. (60 min; 2004). Blanchard et al. (2004) relate the mean time spent

Biogeosciences Discuss., https://doi.org/10.5194/bg-2018-325
Manuscript under review for journal Biogeosciences
Discussion started: 10 July 2018

by cells at the surface to the time at which the photosynthetic capacity at saturating light levels of epipelic diatoms sampled on the same mudflat started to decrease (Blanchard et al., 2004). In our study, the mean time spent by cells at the surface also fluctuates according the total MPB biomass, leading to an inverse relationship with the total MPB biomass. Once at the surface, the simulated MPB growth is regulated by the mass-specific photosynthetic rate in $\mu g\,C\,(\mu g\,chl\,a)^{-1}\,h^{-1}$ converted into a growth rate (h^{-1}) using a variable C:Chl *a* ratio. The resulting MPB growth rates simulated by the model (0.24 ± 0.07 d^{-1} with a range of values between 0.04 d^{-1} and 0.43 d^{-1}) were consistent with observations made on epipelic diatoms (0.035 - 0.86 d^{-1}; Gould and Gallagher, 1990; Underwood and Smith, 1998; Scholz and Liebezeit, 2012). With respect to the simulated C:Chl *a* ratio, it varies in a range of values between 16 and 75.5 $g\,C\,g\,chl\,a^{-1}$ within the range of observed values in mudflats (18.7 - 80 $g\,C\,g\,chl\,a^{-1}$; Guarini, 1998; Gould and Gallagher, 1990; de Jonge et al., 2012).

Contrary to Chl *a* measurements, there were no PP measurements made in 2008 on the Brouage mudflat. For comparison, we use averages of mass-specific photosynthetic rates computed from previous measurements at different locations on the Brouage mudflat for different years (using CO_2 fluxes data measured in benthic chambers). Despite the year-to-year variability, the mean mass-specific photosynthetic rates simulated by the model during spring tides (0.61 ± 0.08 $mg\,C\,(mg\,chl\,a)^{-1}\,h^{-1}$ in April, 0.64 ± 0.12 $mg\,C\,(mg\,chl\,a)^{-1}\,h^{-1}$ in May and 0.43 ± 0.03 $mg\,C\,(mg\,chl\,a)^{-1}\,h^{-1}$ in July) were in the range of measurements for the same months (1.6 ± 1.1 $mg\,C\,(mg\,chl\,a)^{-1}\,h^{-1}$ in April 2012, 0.28 ± 0.11 $mg\,C\,(mg\,chl\,a)^{-1}\,h^{-1}$ in May 2015 and 0.32 ± 0.13 $mg\,C\,(mg\,chl\,a)^{-1}\,h^{-1}$ in July 2015; pers.comm. from J. Lavaud). Morevover, simulated daily and yearly PP rates compared to measurements made across other European intertidal mudflats. The simulated annual ($118\,g\,C\,m^{-2}\,y^{-1}$) and daily mean ($320 \pm 219$ $mg\,C\,m^{-2}\,d^{-1}$) PP rates were in the range of reported estimates ($140 \pm 82\,g\,C\,m^{-2}\,y^{-1}$, N = 18 and 690 ± 682 $mg\,C\,m^{-2}\,d^{-1}$, N = 9, respectively; Underwood and Kromkamp, 1999). The model-data comparison suggests that the model can resolve with confidence the main patterns of the MPB seasonal cycle.

The relative contribution of light, MST and grazing to the simulated MPB seasonal cycle resulted from the coupling of the fortnightly tidal cycle and seasonal solar irradiance and air temperature cycles. Such a coupling is reported in intertidal sediments in the Tagus estuary, Portugal (Serodio and Catarino, 1999). In the model, an emersion period takes place in the middle of the day during spring tides exposing the mud surface to a daily solar irradiance and temperature maximum. In summer, when the seasonal maximum of daily solar irradiance and temperature is reached, the high simulated MST values translate into an enhanced thermo-inhibition of MPB growth and *P. ulvae* grazing pressure. The highest MPB thermo-inhibition in summer spring tides was also highlighted by Guarini et al. (1997) in the Brouage mudflat. During neap tides, light limits the MPB growth when emersion periods occur early in the morning and late in the afternoon at low daily light levels. The reduced PP of MPB at low light levels and MST values during neap tides compared to spring tides was also observed by Kwon et al. (2014) on the Hwaseong mudflat, South Korea.

In the model, we do not consider any MPB limitation by inorganic nutrients. In the Brouage mudflat, Feuillet-Girard et al. (1997) highlighted the greater affinity of MPB to ammonium compared to nitrate. They observed a higher ammonium availability released from the sediment during summer, making unlikely the nutrient limitation responsible of the summer depression of MPB biomass. The high nutrient availability in summer can be attributed to faunal activities (bioturbation, bio-irrigation, excretion; Feuillet-Girard et al., 1997; Heilskov et al., 2006; Laverock et al., 2011; Rakotomalala et al., submitted).

Biogeosciences Discuss., https://doi.org/10.5194/bg-2018-325
Manuscript under review for journal Biogeosciences
Discussion started: 10 July 2018

4.2 Role of mud surface temperature on the MPB and *P. ulvae* activity

On the Brouage mudflat, the simulated MST plays a major role in the MPB seasonal cycle. In spring, the simulated MST increases towards the MPB temperature optimum for photosynthesis (T_{opt}). Along with increasing light levels, it contributes to increase the mass-specific photosynthetic rate and triggers the onset of the MPB spring bloom. As soon as the simulated MST exceeds the MPB temperature optimum for photosynthesis, the MPB PP starts to decrease due to thermo-inhibition, particularly during spring tides. Because of the heat inertia of the surface sediment, the simulated MST decreases in fall slower than the solar irradiance. As a consequence, the simulated MST departs slower from the temperature optimum for photosynthesis than does the downward irradiance from the light saturation parameter (E_k). Despite decreasing solar irradiance in fall, the simulated MPB PP increases until November, when the simulated MPB growth rate is limited by too low light levels and MST values with respect to the MPB light saturation parameter (100 $\mathrm{W\,m^{-2}}$) and temperature optimum for photosynthesis (18 °C), respectively.

Using the Production-Temperature (P-T) model from Blanchard et al. (1996), Blanchard et al. (1997) and Guarini et al. (2006) also suggested that the MPB PP was temperature-limited in summer on the Brouage mudflat. On a southern intertidal mudflat (Tagus Estuary, Portugal), Brito et al. (2013) suggested that thermo-inhibition was responsible for the summer MPB depression observed in NDVI times series in conditions of high sediment temperature (30 °C). In addition, the detrimentral effect of MST ranging between 18 °C and 24 °C was shown in microcosms using fluorescence (Cartaxana et al., 2015).

In the model, the production is related to temperature according the P-T relationship of Blanchard et al. (1996). As a result, the occurrence and intensity of MPB thermo-inhibition depends on the MPB temperature optimum and maximum for photosynthesis used in the relationship. The set of parameters determines the thermal threshold and interval at which thermo-inhibition occurs. The sensitivity analysis shows that the annual PP is very sensitive to the temperature amplitude between the two parameters. The annual PP increases as the amplitude increases. On the Brouage mudflat, the MPB temperature optimum and maximum for photosynthesis were estimated to 25 °C and 38 °C, respectively, and assumed to be constant over the year (Blanchard et al., 1997). In our study, a lower MPB temperature optimum for photosynthesis value of 18 °C is required to simulate a spring bloom that compares to the NDVI time series. Such a temperature optimum also implies a more rapid onset and a higher MPB thermo-inhibition as the simulated MST increases in summer. Values of both MPB temperature optimum and maximum for photosynthesis are reported to vary by up to 10 °C (Table 5). To that respect, the MPB temperature optimum for photosynthesis is a key parameter in the model, because it constrains the onset of the MPB spring bloom and the thermo-inhibition span and intensity.

In addition, the strong heating and wind exposure of the mud surface is accompanied by pore water evaporation that results into desiccation and increased salinity (Coelho et al., 2009). A decrease of pore water content can induce even more detrimental effects within the cells through production of reactive oxygen species (Rijstenbil, 2003; Roncarati et al., 2008) potentially leading to the oxydation of the photosynthetic unit (Nishiyama et al., 2006). The motility of epipelic diatoms is supposed to be a strategy to avoid harmful conditions at the surface of cohesive sediments (Admiraal, 1984). However, Juneau et al. (2015) showed no significant negative effect of salt stress on the photosynthesis of immobile epipelic diatoms. Coelho et al.

(2009) highlighted the role of the rate of pore water content decrease in the field. While slow desiccation (reduction by 40% of the pore water content in 4.5 h) had no significant negative effect on the photosynthesis of microphytobenthic cells within the biofilm, fast desiccation (reduction by 40% of the pore water content in 2 h) resulted in desiccation and decreased the photosynthetic activity of MPB (Coelho et al., 2009). The speed of physiological adaptations by epipelic diatoms to cope with salt stress could be overtaken by the rate of de-watering (Coelho et al., 2009). In addition to micro-migrations, epipelic diatoms produce extracellular polymeric substances (EPS) to temper the effect of desiccation and high salinity (Sauer et al., 2002). High sediment temperature (> 35 °C) is also known to reduce the motility of MPB diatoms and so their capacity to avoid harmful conditions at the sediment surface (Cohn et al., 2003; Laviale et al., 2015). To that respect, the use in the model of a MPB temperature optimum for photosynthesis lower than values reported in the litterature (Table 5) may overestimate the thermo-inhibition process and, as such, promote low PP rates. Nevertheless, this negative feedback on PP may compensate the absence in the model of detrimental effects of desiccation on the microphytobenthic cells, which is a positive feedback on PP.

The simulated MST also rules the ingestion rate of MPB by the grazer *P. ulvae* in the model. The grazing parameters play an important role in the regulation of MPB annual production. Simulated PP rates increase as the value of the optimal temperature for grazing increases because the grazing optimum is not often reached in the model. Meanwhile, simulated PP rates decrease with augmentation of the shape parameter of the temperature-related grazing (α_Z) because of the increase of the grazing exponential terms resulting into a higher simulated grazing pressure. In the model, the ingestion rate increases when the MST exceeds the optimal temperature for grazing (fixed at 20 °C; Pascual and Drake, 2008). A high metabolism of benthic grazers promoted by high temperature conditions (up to 22 °C) and the resulting increase of the grazing pressure on benthic diatoms was observed by Sahan et al. (2007) on a mudflat in Netherlands.

In the model, we report 49 days in 2008 during which the simulated MST daily averaged over the emersion periods exceeded the optimal temperature for grazing (T_{opt_Z}, 20 °C). However, the simulated grazing pressure results into a decrease of the MPB PP for only 11 days. The remaining 38 days, grazing did not exceed the MPB PP. Such a behavior of the model highlights the key role played by the MST in simulating the MPB and *P. ulvae* growth rates. It also suggests that the seasonal MPB dynamics is likely to be strongly impacted by the interannual variability of the meteorological conditions (de Jonge et al., 2012; Benyoucef et al., 2014), which regulates the simulated bottom-up (i.e. MPB thermo-regulation) and top-down (i.e. grazing) processes.

4.3 Effect of light on MPB photosynthesis

In the model, light is the most limiting factor throughout the year. The low irradiance during fall and winter limits the MPB photosynthesis as the irradiance is in average lower than the light saturation parameter (E_k). In spring, the increasing irradiance and MST translate into higher mass-specific photosynthetic rates than in fall-winter leading to the onset of the simulated MPB spring bloom. In summer, photo-inhibition is not accounted for in the model as the simulated mean time spent by a MPB cells at the surface is lower than the time required to induce photo-inhibition at saturating light levels (Blanchard et al., 2004). As a consequence, light limits the simulated MPB growth only during neap tides, when the sediment emersion occurs at low light levels early and late in the day.

Biogeosciences Discuss., https://doi.org/10.5194/bg-2018-325
Manuscript under review for journal Biogeosciences
Discussion started: 10 July 2018

Photosynthesis is represented in the model by the Production-Irradiance (P-E) model of Platt and Jassby (1976). It relies on the photosynthetic capacity (P^b_{max}), the light saturation parameter (E_k) and the maximum light utilization coefficient ($\alpha = \frac{P^b_{max}}{E_k}$, Talling, 1957). Irradiance has no influence on the photosynthetic capacity and maximum light utilization coefficient (MacIntyre et al., 2002) in our study. Based on the work of (Blanchard et al., 1996), the photosynthetic capacity and maximum light utilization coefficient vary in the model with the simulated MST. Therefore, the seasonal adjustment of photosynthesis to irradiance depends mainly on the photoacclimation status of MPB cells, which can be related to the light saturation parameter (Sakshaug et al., 1997). The light saturation parameter corresponds to the irradiance at which photosynthesis switches from light reactions (light absorption and photochemical energy conversion) to dark reactions (reductant utilization) (Sakshaug et al., 1997). It has been reported to vary seasonally in benthic microalgae (Blanchard and Cariou-Le Gall, 1994; Barranguet et al., 1998; Light and Beardall, 2001; Pniewski et al., 2015; Barnett et al., 2015). Cells increase their light saturation parameter at high irradiance (summer) and reduce it with decreasing light levels (Sakshaug et al., 1997). In our study, as the light saturation parameter is set as constant throughout the year (100 $\mathrm{W\,m^{-2}}$), photoacclimation is simulated by the way of a variable C:Chl *a* ratio.

During winter, low light acclimated cells have a lower C:Chl *a* ratio due to an increase of the Chl *a* content (MacIntyre et al., 2002; Brunet et al., 2011). In summer, with the increasing irradiance and day length, high light-acclimated cells reduce their Chl *a* content leading to a higher C:Chl *a* ratio (MacIntyre et al., 2002; Brunet et al., 2011). In the model, solar irradiance shapes the simulated C:Chl a ratio (Eq. B9 in Appendix B2). The C:Chl *a* ratio reaches a seasonal maximum value (75.5 $\mathrm{g\,C\,g\,chl}\,a^{-1}$) in summer when solar irradiance is the highest. Such a result is consistent with estimate (80 $\mathrm{g\,C\,g\,chl}\,a^{-1}$) reported in summer by de Jonge et al. (2012). In the model, given that the mass-specific photosynthetic rate (µg C $(\mu\mathrm{g\,chl}\,a)^{-1}\,\mathrm{h}^{-1}$) and the C:Chl *a* ratio are related to the growth rate (h^{-1}), the growth rate increases as the C:Chl *a* ratio decreases (low light acclimated cells). The seasonal variation of the simulated growth rate results from the combination of the variation of the photosynthetic capacity and maximum light utilization coefficient driven by the simulated MST and the variation of the C:Chl *a* ratio with irradiance.

Finally, photoinhibition at high irradiance is not accounted for in the P-E model of Platt and Jassby (1976) used in the model. Epipelic diatoms achieve "micro-migrations" within the sediment to avoid harmful light conditions prevailing at the sediment surface (Kromkamp et al., 1998; Perkins et al., 2001; Cartaxana et al., 2011). However, combined with high temperature conditions (> 35 °C) at the sediment surface potentially leading to reduced cell motility (Cohn et al., 2003), epipelic diatoms can be photoinhibited (Laviale et al., 2015). In temperate intertidal mudflats, high light and temperature conditions occur during summer and their combined effect on MPB photosynthetic rate may explain the depression of MPB biomass observed in summer.

4.4 Top-down regulation of MPB dynamics

Grazing by meio- and macrobenthos is often suggested as the main driver of the MPB biomass depression observed in summer on intertidal mudflats (Cadée and Hegeman, 1974; Cariou-Le Gall and Blanchard, 1995; Sahan et al., 2007; Orvain et al., 2014). Weerman et al. (2011) showed experimentally a strong decrease of MPB biomass in the presence of macrofauna driven by direct grazing and by the absence of surface mud stabilisation due to bioturbation by deposit feeders.

Biogeosciences Discuss., https://doi.org/10.5194/bg-2018-325
Manuscript under review for journal Biogeosciences
Discussion started: 10 July 2018

In the model, *P. ulvae* grazing exceeds the MPB PP mainly in summer. The simulated grazing pressure corresponds to 6 synoptic events (between 1 and 4 days) of MPB biomass removal when the MST is higher than the temperature optimum for grazing. 90 % of these events occurs when the simulated MPB growth is already temperature-limited as the temperature optimum for grazing is higher than the temperature optimum for photosynthesis. Consequently, the grazing pressure by *P. ulvae* adds to the effect of thermo-inhibition. Throughout 2008, such a combined effect takes place 2.7 % of the year. The simulated gain terms promoting the growth rate of MPB limited by thermo-inhibition do not compensate the loss terms dominated by the grazing pressure, which leads to a decrease of the MPB biomass. In a schematic model, Thompson et al. (2000) showed such a seasonal uncoupling between the grazing intensity by intertidal grazing molluscs and the microalgae abundance from observations made on a rocky shore of the Isle of Mann (United Kingdom). The authors conceptualized the role played by the light and temperature stress on the microalgae productivity and by the temperature-promoted grazing in the depression of the microalgal standing stocks in summer.

The combined effect of grazing and thermo-inhibition translates into 14 % (15.8 $\mathrm{g\,C}$) of the simulated annual MPB PP channeled towards the *P. ulvae* and secondary production. The simulated gross *P. ulvae* secondary production is 13.63 $\mathrm{g\,C\,m^{-2}\,y^{-1}}$, which represents 11.5 % of the simulated annual MPB PP (118 $\mathrm{g\,C\,m^{-2}\,y^{-1}}$). This fraction of PP transferred to *P. ulvae* secondary production is consistent with the average fraction reported by Asmus and Asmus (12.5 %; 1985) on intertidal sand bottom communities of the Island of Sylt in the North Sea.

In July, the simulated density of *P. ulvae* lies in the lower range of time-coincident measurements. As the simulated MST fairly agrees with time-coincident measurements, other factors may explain the likely underestimation by the model of the density and ingestion of *P. ulvae*. First, there may be a bias resulting from the monthly mean weight estimates used to simulate the *P. ulvae* density (see Appendix B3). The monthly mean weights are based on samples gathered in 2014-2015 on the Aiguillon mudflat, in the vicinity of the Brouage mudflat (Fig. 1). Nevertheless, the seasonality of the *P. ulvae* density is similar on the two mudflats with a peak of density in late summer (Haubois et al., 2002), which suggests that such a bias is likely limited. In addition, apart from the four events of high ingestion, the simulated ingestion rates (0 - 50 $\mathrm{ng\,chl\,}a\,\mathrm{ind^{-1}\,h^{-1}}$) are consistent with ingestion rates measured in experiments with *P. ulvae* and benthic diatoms collected in our study area and performed at temperature close to the optimal temperature for grazing in the model (15 - 20 °C; 0.75 - 52 $\mathrm{ng\,chl\,}a\,\mathrm{ind^{-1}\,h^{-1}}$; Blanchard et al., 2000; Haubois et al., 2005; Pascal et al., 2008). Concerning simulated peaks of ingestion, the maximum ingestion rate (334 $\mathrm{ng\,chl\,}a\,\mathrm{ind^{-1}\,h^{-1}}$) simulated during the peak of July 22 is coherent with the maximum ingestion rate (385 $\mathrm{ng\,chl\,}a\,\mathrm{ind^{-1}\,h^{-1}}$) experimentally measured by Coelho et al. (2011) in Portugal. Second, the wave- and tidal-induced shear stress on the bottom sediment may transport horizontally *P. ulvae* individuals across the mudflat. Such a process is not accounted for in the model and may lead to an underestimation of the *P. ulvae* biomass and density. Finally, potential MPB grazing by fauna other than *P. ulvae* is represented in a simple way by a linear and generic loss term in the model whereas it might be a non-linear process that can vary seasonally (Pinckney et al., 2003). This closure term may be underestimated in the model.

With respect to meiofauna, Pinckney et al. (2003) suggested a more intense grazing by meiofauna in summer than in winter in the Terrebonne Bay estuary (USA). Admiraal et al. (1983) estimated the meiofauna grazing at 300 $\mathrm{mg\,C\,m^{-2}\,d^{-1}}$ on a mudflat

of the Ems Dollard estuary (Netherlands). Comparable rates of meiofauna ingestion (58 - 189 $\mathrm{mg\,C\,m^{-2}\,d^{-1}}$) are reported for the Brouage mudflat (Montagna et al., 1995). Admiraal et al. (1983) concluded to a non significant effect of meiofauna grazing relative to the MPB production rates they measured. Nevertheless, their estimated grazing rate exceeds our simulated daily MPB production rates for 26 days in summer i.e. 29% of the time of the second phase in the model, suggesting that meiofauna grazing could impact MPB. In addition, Pascal et al. (2008) compared ingestion rates by *P. ulvae* and a nematode community from the Brouage mudflat in experimental conditions. According to the abundance of organisms selected for the experiment of Pascal et al. (2008) and a constant C:Chl *a* ratio of 45 $\mathrm{g\,C\,g\,chl}\,a^{-1}$ (Guarini, 1998), the amount of Chl *a* ingested by nematodes per hour was only 1.5 % of the Chl *a* ingested by *P. ulvae* per hour in their experiment. However, in regard to the observed abundances on the field and without density-dependant effect on grazing rates, this theoritical amount of Chl *a* ingested by nematodes increases to almost 50% of the Chl *a* ingested by *P. ulvae* in the study of Pascal et al. (2008). According to the measured biomass uptake by meiofauna (Montagna et al., 1995) and nematodes (Pascal et al., 2008) for the Brouage mudflat, an explicit representation of meiofauna ingestion in the model might magnify the simulated depletion of MPB biomass in summer months. The representation of grazing in the model can be improved. Nevertheless, the fair agreement between the simulated *P. ulvae* densities and biomass levels with time-limited but time-coincident observations suggests that overall the model simulates with some confidence the grazing pressure on MPB.

4.5 Physical setting of the coupled model

The predictive ability of the physical-biological coupled model depends on the accuracy of the oceanic and meteorological forcings. The frequency of the water height and meteorological time series used to constrain the model is hourly while the model time step is 06 minutes. The lower frequency of the model forcings over a day partly explains the model-data discrepancies. In addition, the weather station where meteorological data were acquired is located 30 km away from the Brouage study site. Local weather conditions may differ between the two sites, especially the global irradiance and wind speed used to simulate the MST and MPB growth rate. Global irradiance can be impacted by local cloud cover and the wind regime can be different due to local thermal winds. In the model, the timing of the emersion-immersion cycle is constrained by the observed water heights and bathymetric level. The bathymetric level used to compute the water height above the Brouage study site originates from a digital elevation model with a 1-m horizontal resolution and a 15-cm vertical precision. Even if the Brouage mudflat is relatively flat (1:1000), ridges and runnels are present near the study site (Gouleau et al., 2000) and the topography is highly variable at a meter scale. Inaccuracies in the bathymetric level relative to the study site may translate into model-data discrepancies in terms of timing of the emersion-immersion cycle in the model. Given that the mud temperature model is constrained by the water height and meteorological data, it is sensitive to possible inaccuracies in the forcings that may impact the simulated hourly dynamics of MPB and *P. ulvae*. Nevertheless, at the seasonal scale, the impact on the biological compartments of such inaccuracies in the forcings may be limited.

Biogeosciences Discuss., https://doi.org/10.5194/bg-2018-325
Manuscript under review for journal Biogeosciences
Discussion started: 10 July 2018

5 Conclusion and perspectives

This study is a first attempt to simulate the MPB seasonal cycle observed on a temperate intertidal mudflat and to quantify the relative contribution of both biotic and abiotic factors on the seasonal MPB dynamics. The physical-biological coupled model fairly compares to time-coincident remotely sensed and *in situ* data and provides key findings about the seasonality of MPB on the Brouage mudflat (French Atlantic coast):

- The 2008 MPB seasonal cycle consists in 3 phases: a spring bloom, a summer depression of the biomass levels, and a moderate peak of biomass in fall;
- In winter and early spring, the seasonal mass-specific maximum photosynthetic rate mainly driven by the simulated MST and the seasonal low C:Chl *a* ratios lead to a seasonal maximum of MPB growth rate and to a MPB spring bloom;
- Thermo-inhibition (39.5 % of summer) and *P. ulvae* grazing (8.7 % of summer) are responsible for the MPB biomass depression occurring in summer. Grazing exceeds the MPB PP 90 % of the time when the MPB growth is already temperature-limited;
- The combined effect of grazing and thermo-inhibition results into 14 % of the simulated annual MPB primary production channeled towards the *P. ulvae* secondary production through ingestion;
- The model is sensitive to MPB temperature parameters (temperature optimum and maximum for photosynthesis), to the MPB light saturation parameter and, to a lesser extent, to grazing parameters (the optimal temperature for grazing and the shape parameter of the temperature-related grazing function).

The seasonal MPB dynamics simulated by the model compares to time coincident times series of remotely sensed NDVI data hence providing a qualitative assessement of the model predictive ability. A next step would be to extend such a model-satellite data comparison to a more quantitative assessment to validate the simulated levels of MPB Chl *a* concentration and PP. The recent advance of multispectral and hyperspectral remote sensing allows for the development of new algorithms to retrieve products of ecological interest for MPB. Brito et al. (2013) developed local empirical relationships relating synchronized NDVI data to *in situ* Chl *a* concentrations to retrieve from space estimates of Chl *a* concentration on a Portugese intertidal mudflat. Efforts are also focused in using remote sensing reflectances from airbone hyperspectral data to assess MPB PP rates (Méléder et al., 2018). Recently, and in the light of the work of Brito et al. (2013), Daggers et al. (2018) combined biomass derived from NDVI data with simulated photosynthetic capacity from environmental conditions (irradiance and air temperature) to map MPB PP on intertidal mudflats in Netherlands. Other promising methods in the estimation of PP in intertidal mudflat at the ecosystem scale are the non-invasive atmospheric and aquatic Eddy Covariance (EC) techniques. The atmospheric EC provides continuous and direct CO_2 flux measurements at the air-water and air-sediment interfaces during high and low tides, respectively, across different time scales from hours to years (Baldocchi et al., 1988; Aubinet, Marc and Grelle, Achim and Ibrom, Andreas and Rannik, Üllar and Moncrieff, John and Foken, Thomas and Kowalski, Andy S and Martin, Philippe H and Berbigier, Paul and Bernhofer, Ch and others, 1999; Zemmelink et al., 2009; Polsenaere et al., 2012). Similarly, the aquatic

EC measures benthic O_2 fluxes at the sediment/water interface (Berg et al., 2003). Quantifying the MPB PP and biomass on intertidal mudflats is a prerequisite for further estimating the flux of biogenic carbon from the benthos to the pelagos. During the immersion period, MPB can be resuspended (9.7 $\mathrm{mg\,C}$ per high tide, i.e 3 % of the mean simulated production during low tides, Dupuy et al., 2014) and highly disturb the functionning of the benthic-pelagic ecosystem (Saint-Béat et al., 2014). The study of air-water and sediment-water exchanges through simultaneous atmospheric and aquatic EC measurements could allow quantifying the importance of metabolic fluxes during immersion and emersion periods but also the coupled processes between the benthic and pelagic compartments such as MPB resuspension. Microphythobenthic community resuspension can significantly contribute to planktonic gross PP and, in turn, explain lower CO_2 fluxes from the water column to the atmosphere at high tide during the day than at night (Guarini et al., 2008; Polsenaere et al., 2012). To date, the modelling effort put on the physically-driven (tides and waves) resuspension processes of MPB is still limited (see Mariotti and Fagherazzi, 2012). Accounting in models for sediment bottom shear stress mediated by hydrological forcings (current and waves) along with bioturbation processes could lead to more realistic predictions of the interannual MPB dynamics. Such a representation of the biologically and physically-driven benthic-pelagic interactions would be fully apprehended by the coupling of biological MPB models to high resolution ocean models. Such an approach would open the door to an accurate assessement of the vertical and horizontal export flux of biogenic matter at the land-ocean interface and, more generally, of the contribution of productive biofilms in mudflats in the carbon cycle of the global coastal ocean.

Code availability.

Data availability.

Code and data availability.

Appendix A: Mud temperature model

The original version of the mud temperature model of Guarini et al. (1997) is simplified by only resolving the mud surface temperature $T_M\,(z_0,t)$ (K) which is governed by the following equation:

$$\rho_M C_{P_M} \frac{\partial T_M\,(z_0,t)}{\partial t} = f\,(T_M(z_0,t))\,, \tag{A1}$$

where $f\,(T_M(z_0,t))$ is the heat energy balance (HEB, $\mathrm{W\,m^{-2}}$) at the sediment surface z_0 (m) at time t (s). This sediment surface layer is 1-cm deep. The temperature (K) is assumed to be homogenous within the layer and is governed by the HEB (Harrison and Phizacklea, 1987; Piccolo et al., 1993). ρ_M is the volumetric mass of mud ($\mathrm{kg\,m^{-3}}$). It is the sum of the water fraction and of the dry sediment fraction ($\rho_M = \rho_W \xi + \rho_S(1-\xi)$ where ρ_W and ξ are the water volumetric mass ($\mathrm{kg\,m^{-3}}$)

Biogeosciences Discuss., https://doi.org/10.5194/bg-2018-325
Manuscript under review for journal Biogeosciences
Discussion started: 10 July 2018

and the porosity (%), respectively. C_{P_M} is the specific heat capacity of mud at constant pressure ($\mathrm{J\,kg^{-1}\,K^{-1}}$):

$$C_{P_M} = \frac{\eta}{\mu\rho M}, \tag{A2}$$

where η is the heat conductivity ($\mathrm{W\,m^{-1}\,K^{-1}}$) and μ the thermal diffusivity ($\mathrm{m^2\,s^{-1}}$). Heat exchange fluxes at the sediment interface are different according to the emersion-immersion cycle. During low tide, the HEB is governed by downward fluxes of radiation from the sun (R_S, $\mathrm{W\,m^{-2}}$) and from the atmosphere (R_{Atm}, $\mathrm{W\,m^{-2}}$), by upward fluxes of radiation from the receiving surface (R_M, $\mathrm{W\,m^{-2}}$), by sensible heat fluxes by conduction due to mud-air temperature difference ($S_{Mud\rightarrow Air}$, $\mathrm{W\,m^{-2}}$) and by flux of evaporation (V_M, $\mathrm{W\,m^{-2}}$):

$$f\left(T_M(z_0,t)\right) = R_S + R_{Atm} - R_M - S_{Mud\rightarrow Air} - V_M \text{ with } V_M = \xi V_W, \tag{A3}$$

where ξ is the mud porosity ($\xi \in [0,1]$, %) and V_W the evaporative heat flux of seawater ($\mathrm{W\,m^{-2}}$). Details about formulas and constants computation of each fluxes during emersion are given in Tables A1 and A2. During immersion, only a sensible heat flux from seawater to mud is taken into account because the overlying turbid seawater is assumed to limit the penetration of the downward irradiance (Harrison and Phizacklea, 1985; Losordo and Piedrahita, 1991). The sensible heat flux consists in the product of the conductivity and with a finite-difference approximation of the temperature gradient between mud and the overlying seawater (Losordo and Piedrahita, 1991):

$$f\left(T_M(z_0,t)\right) = S_{Mud\rightarrow Water} = -\frac{\eta}{h_W}\left(T_M\left(z_0,t\right) - T_W(t)\right) \text{ with } h_W = 0.2H, \tag{A4}$$

where h_W corresponds to the the overlying water mixing height (m), a fraction of the total height (H in m). The seawater temperature (T_W) is computed according to the heat exchange through heat conduction within the surface mixed layer ($z_{\alpha_{MLD}}$):

$$T_W(t) = \alpha_{MLD} T_W(z_{\alpha_{MLD}},t) + (1-\alpha_{MLD})\,T_W(t) \text{ with } \alpha_{MLD} = 0.12\left(1+\frac{U}{3}\right) \tag{A5}$$

where $T_W(z_{\alpha_{MLD}},t)$ is the water temperature in the surface mixed layer (K). α_{MLD} is the depth of the mixed layer (m) according the wind speed U ($\mathrm{m\,s^{-1}}$). The surface water temperature is also governed by the HEB at the water surface:

$$\rho_W C_{P_W} \frac{\partial T_W\left(z_{\alpha_{MLD}},t\right)}{\partial t} = f\left(T_W(z_{\alpha_{MLD}},t)\right), \tag{A6}$$

$$\text{with } f\left(T_W(z_{\alpha_{MLD}},t)\right) = R_S + R_{Atm} - R_W - S_{Air\rightarrow Water}, \tag{A7}$$

where ρ_W is the volumetric mass of water ($\mathrm{kg\,m^{-3}}$). C_{P_W} is the specific heat capacity of seawater at constant pressure ($\mathrm{J\,kg^{-1}\,K^{-1}}$). The term $S_{Air\rightarrow Water}$ is the sensible heat flux mediated by thermal conduction due to water-air temperature difference. R_W ($\mathrm{W\,m^{-2}}$) is the seawater upward radiation. T_W (K) is initiliazed by the following equation:

$$T_W(t) = 17 + 5cos\left(2\pi\frac{day-230}{year\ length}\right) + 273.15 \tag{A8}$$

where day is the day of the year and the year length is in days. Details on parameters and constants are given in Tables A1 and A2.

Biogeosciences Discuss., https://doi.org/10.5194/bg-2018-325
Manuscript under review for journal Biogeosciences
Discussion started: 10 July 2018

Appendix B: Biological model

B1 MPB migration scheme

A system of three partial differential equations describes the temporal dynamics of the MPB biomass within the surface biofilm (S), MPB biomass within the 1st cm of sediment (F), and biomass of MPB grazer *P. ulvae* (Z). The system drives the MPB migration scheme according to the diurnal and tidal cycles that constrain the biological-physical coupled model (Table 1). During the daytime emersion period:

$$\text{if } \tau > 0 \begin{cases} \frac{dS}{dt} = \left(r_F F + P^b S\right)\left(1 - \frac{S}{S_{max}}\right) - m_S S - min\left[IR\left(\frac{Z}{W_Z^{mean}}\right), S_{IR}\right] \times H\left(F, F_{mini}\right) \\ \frac{dF}{dt} = -r_F F\left(1 - \frac{S}{S_{max}}\right) + P^b S\left(\frac{S}{S_{max}}\right) - m_F F \\ \frac{dZ}{dt} = \gamma \times min\left[IR\left(\frac{Z}{W_Z^{mean}}\right), S_{IR}\right] \times H\left(F, F_{mini}\right) - m_Z Z \\ \frac{d\tau}{dt} = -1 \end{cases} \tag{B1}$$

$$\text{if } \tau \leq 0 \begin{cases} \frac{dS}{dt} = -r_S S - m_S S - min\left[IR\left(\frac{Z}{W_Z^{mean}}\right), S_{IR}\right] \times H\left(F, F_{mini}\right) \\ \frac{dF}{dt} = r_S S - m_F F \\ \frac{dZ}{dt} = \gamma \times min\left[IR\left(\frac{Z}{W_Z^{mean}}\right), S_{IR}\right] \times H\left(F, F_{mini}\right) - m_Z Z \\ \frac{d\tau}{dt} = -1 \end{cases} \tag{B2}$$

where τ (h) corresponds to the potential duration of the biofilm or the potential duration of the production period. It is computed at the end of each nighttime emersion and immersion periods for the next daytime emersion period (Eq. B4 and B6). When $\tau > 0$, the MPB cells migrate upward in the sediment from F to S compartment at a transfer rate of r_F (h^{-1}). MPB stop migration when S reaches saturation at S_{max} ($\mathrm{mg\,chl}\,a\,\mathrm{m}^{-2}$). Primary production within the S compartment regulated by the mass-specific photosynthetic rate P^b ($\mu\mathrm{g\,C}\,(\mu\mathrm{g\,chl}\,a)^{-1}\,\mathrm{h}^{-1}$) is set to zero when $S = S_{max}$ according to the term $\left(1 - \frac{S}{S_{max}}\right)$, which represents the MPB space-limitation in S compartment. The MPB biomass produced is therefore tranferred from S to F according to the term $P^b S\left(\frac{S}{S_{max}}\right)$ in the F time derivative. In order to take into account for all the MPB biofilm biomass plus the biomass produced in the biofilm ($S*$), the $S*$ time derivative was computed as follows:

$$\frac{dS*}{dt} = \frac{dS}{dt} + \boldsymbol{P^b S}\left(\frac{\boldsymbol{S}}{\boldsymbol{S_{max}}}\right). \tag{B3}$$

When $\tau \leq 0$, the MPB cells migrate downward in the sediment from the S to F compartment at a transfer rate of r_S (h^{-1}). The terms m_S and m_F are loss rates (h^{-1}) repesenting MPB senescence and grazing by surface deposit feeders (on S) and subsurface deposit feeders (on F). m_Z is a loss rate (h^{-1}) representing *P. ulvae* senescence (see Appendix B3).

Biogeosciences Discuss., https://doi.org/10.5194/bg-2018-325
Manuscript under review for journal Biogeosciences
Discussion started: 10 July 2018

During the night emersion period, the MPB cells migrate downward into the sediment from S to F. *P.ulvae* grazes on MPB cells remaining in the biofilm (S):

$$\begin{cases} \frac{dS}{dt} = -r_S S - m_S S - min\left[IR\left(\frac{Z}{W_Z^{mean}}\right), S_{IR}\right] \times H\left(F, F_{mini}\right) \\ \frac{dF}{dt} = r_S S - m_F F \\ \frac{dZ}{dt} = \gamma \times min\left[IR\left(\frac{Z}{W_Z^{mean}}\right), S_{IR}\right] \times H\left(F, F_{mini}\right) - m_Z Z \\ \tau = \left(\frac{F}{S_{max}} + 1\right) \times \tau_s \end{cases} \quad \text{(B4)}$$

According to Guarini et al. (2006, 2008), τ depends on the MPB biomass in the F compartment relative to S_{max} and on the average time spent at the surface by a unit of biomass equal to S_{max} (τ_s, h). It suggests the higher is the biomass in F, the longer S will remain at saturation S_{max}. In order to obtain a MPB density-dependant effect, τ_s is mediated by the ratio of F to a carrying capacity (F_{max}):

$$\tau_s = \tau_{s_{max}} \left[max\left(1 - \left(\frac{F}{F_{max}}\right), \tau_{s_{min}}\right)\right] \quad \text{(B5)}$$

$\tau_{s_{max}}$ (1 h, Blanchard et al., 2004) is the maximum time spent at the surface by a unit of biomass equal to S_{max}. $\tau_{s_{min}}$ is the minimum value of τ_s set at 0.02 h. It is set according the minimum time τ needed to obtain a saturating biofilm i.e. 15 min (Herlory et al., 2004). From now on, the higher is F, the lower is the time period during which the biofilm is at the saturation level.

During the immersion period, MPB cells remaining in the biofilm finish their downward migration and *P. ulvae* does not exert any grazing pressure anymore:

$$\begin{cases} \frac{dS}{dt} = -r_S S - m_S S \\ \frac{dF}{dt} = r_S S - \nu_F F \\ \frac{dZ}{dt} = -m_Z Z \\ \tau = \left(\frac{F}{S_{max}} + 1\right) \times \tau_s \end{cases} \quad \text{(B6)}$$

In addition to m_S and m_F, ν_F is a loss rate (h^{-1}) that represents MPB cells senescence plus the chronic resuspension of MPB cells in the water column during immersion periods. Guarini et al. (2006, 2008) used to set S to zero at the beginning of immersion periods. The authors considered that all the remaining cells at the surface were resuspended. In our study, the chronic resuspension of MPB cells from the F compartment to the implicit water column is simulated using a higher loss rate (ν_F) compared to losses during emersion (m_S and m_F) instead of a potential biofilm complete resuspension. Parameter values are given in Table A3.

B2 MPB primary production

The mass-specific photosynthetic rate P^b (µg C (µg chl a)$^{-1}$ h^{-1}) is regulated by temperature (T, °C) and by photosynthetically active radiation (E, W m^{-2}), which corresponds to 44 % of downward shortwave radation (Britton and Dodd, 1976). The

Biogeosciences Discuss., https://doi.org/10.5194/bg-2018-325
Manuscript under review for journal Biogeosciences
Discussion started: 10 July 2018

model of Platt and Jassby (1976) is used to determine the production rate as a function of light:

$$P^b = P^b_{max} \times tanh\left(\frac{E}{E_k}\right), \tag{B7}$$

where P^b_{max} is the photosynthetic capacity ($\mu g\,C\,(\mu g\,chl\,a)^{-1}\,h^{-1}$) and E_k is the light saturation parameter ($W\,m^{-2}$). P^b_{max} depends on the mud surface temperature T according to the relationship of Blanchard et al. (1996):

$$P^b_{max} = P^b_{MAX} \times \left(\frac{T_{max} - T}{T_{max} - T_{opt}}\right)^{\beta} \times e^{\left(-\beta \times \left[\frac{T_{max}-T}{T_{max}-T_{opt}} - 1\right]\right)}, \tag{B8}$$

where T_{max} (°C) and T_{opt} (°C) are the maximum and optimal temperature for the photosynthesis, respectively. β is a curvature coefficient that shapes the temperature-photosynthesis relationship. P^b_{MAX} is the maximum value that takes P^b_{max} at T_{opt}.

The mass-specific photosynthetic rate P^b is expressed in $\mu g\,C\,(\mu g\,chl\,a)^{-1}\,h^{-1}$. It is therefore necessary to convert it in terms of produced Chl *a* to obtain a growth rate in h^{-1}. To that respect, we used a variable C:Chl *a* ratio ($g\,C\,g\,chl\,a^{-1}$) on the finding of de Jonge et al. (2012) on MPB. The ratio is computed according the formulation of Cloern et al. (1995) adapted for coastal pelagic diatoms (Sibert et al., 2010, 2011; Le Fouest et al., 2013):

$$\frac{Chla}{C} = \left(\frac{Chla}{C}\right)_{min} \times \left(1 + 4 \times e^{-0.5 \times \frac{E}{K_E}}\right), \tag{B9}$$

where $\left(\frac{Chla}{C}\right)_{min}$ is the minimum Chl *a*:C ratio ($g\,chl\,a\,g\,C^{-1}$) and K_E, the half-saturation constant for light use (in $Ein\,m^{-2}\,d^{-1}$).

The MPB primary production ($\mu g\,C\,m^{-2}\,h^{-1}$) corresponds to the sum of the space-dependant production at the surface of the biofilm (*i.e.* the $P^b S\left[1 - \frac{S}{S_{max}}\right]$ term) and of the biomass produced and directly transfered from S to F (*i.e.* the $P^b S\left[\frac{S}{S_{max}}\right]$ term). Consequently, it can be simplified by:

$$production = P^b S\left(1 - \frac{S}{S_{max}}\right) + P^b S\left(\frac{S}{S_{max}}\right) = P^b S \tag{B10}$$

The constants values are given in Table A3.

B3 Grazer *P. ulvae*

S is explicitely grazed by the mud snail *Peringia ulvae* (Z, $mg\,C\,m^{-2}$). The grazing rate is regulated by the individual ingestion rate of snails (IR, $ng\,chl\,a\,ind^{-1}\,h^{-1}$) and Z expressed in terms of density ($ind\,m^{-2}$). Density is computed as the ratio of Z ($mg\,C\,m^{-2}$) over the mean individual weight (W_Z^{mean}, $mg\,C$) linearly interpolated on simulation time scale (6 min, Table A4). Grazing rate can not exceed the biomass in S per hour (S_{IR}, $mg\,chl\,a\,m^{-2}\,h^{-1}$) by means of the minimum function $min\left[IR\left(\frac{Z}{W_Z^{mean}}\right), S_{IR}\right]$. The grazing is also limited through a heavyside function (H) including a feeding threshold (F_{mini}, $mg\,chl\,a\,m^{-2}$). Only a fraction (γ, %) of the MPB biomass grazed by Z is assimilated into new Z biomass.

The individual ingestion rate ($ng\,chl\,a\,ind^{-1}\,h^{-1}$) by *P. ulvae* is calculated according to the formulation of Haubois et al. (2005) for adult snails. It depends on the total MPB biomass and on the mud surface temperature:

$$IR = min\left(0.015 \times (F+S)^{1.72} \times e^{\alpha_Z (T - T_{opt_Z})}, IR_{max}\right), \tag{B11}$$

where T_{opt_Z} (°C) is the optimal temperature for grazing. IR_{max} is the maximal observed individual ingestion rate. α_Z (no unit) is a curvature parameter. The Chl *a* uptake is converted into carbon unit according to the C:Chl *a* ratio described previously. The term $(F + S)$ is expressed in µg g dry sed^{-1}. The biomass expressed in $\mathrm{mg\,chl\,}a\,\mathrm{m}^{-2}$ is converted into µg g dry sed^{-1} as follows:

$$[Chla]\,(\text{µg g dry sed}^{-1}) = \frac{[Chla]\,(\mathrm{mg\,chl\,}a\,\mathrm{m}^{-2})}{\varphi} \times thickness_{sed}, \tag{B12}$$

where φ is the sediment bulk density in $\mathrm{g\,l}^{-1}$ and $thickness_{sed}$ is the sediment thickness i.e. $1\ \mathrm{cm}$. Finally, the mortality rate of Z is a quadratic density-dependant mortality rate:

$$m_Z = m_Z^{min} Z, \tag{B13}$$

where m_Z^{min} is the minimum mortality rate (h^{-1}). The constants values are given in Table A3.

Author contributions.

Competing interests. The authors declare that they have no conflict of interest.

Disclaimer.

Acknowledgements. This research was funded by the Centre national d'études spatiales (CNES), the Centre National de la Recherche Scientifique (CNRS, LEFE-EC2CO program), the Région Nouvelle-Aquitaine and the European Union (CPER/FEDER) and the Groupement d'Intérêt Public (GIP) Seine-Aval PHARESEE project. RS was supported by a PhD fellowship from the French Ministry of Higher Education, Research and Innovation. The authors acknowledge Meteo France for providing meteorological data and the Institut National de l'Information Géographique et Forestière (IGN) and the Service Hydrographique et Océanographique de la Marine (SHOM) for providing the digital elevation model of Charente Maritime LITTO3D®. We thank Johann Lavaud (UMI Takuvik, CNRS & Université Laval, Canada) for providing primary production data from measurements made at the study site in 2012 and 2015. We also thank Thierry Guyot (LIENSs) for his help in designing Fig. 2. This research is part of fulfillment of the requirements for a PhD degree (RS) at the Université de La Rochelle, France.

Biogeosciences Discuss., https://doi.org/10.5194/bg-2018-325
Manuscript under review for journal Biogeosciences
Discussion started: 10 July 2018

References

Admiraal, W.: The ecology of estuarine sediment inhabiting diatoms, Progress in Phycological Research, 3, 269–314, 1984.

Admiraal, W., Bouwman, L. A., Hoekstra, L., and Romeyn, K.: Qualitative and quantitative interactions between microphytobenthos and herbivorous meiofauna on a brackish intertidal mudflat, International Review of Hydrobiology, 68, 175–191, 1983.

Asmus, H.: Benthic grazers and suspension feeders: Which one assumes the energetic dominance in Königshafen?, Helgoländer Meeresuntersuchungen, 48, 217, 1994.

Asmus, H. and Asmus, R.: The importance of grazing food chain for energy flow and production in three intertidal sand bottom communities of the northern Wadden Sea, Helgoländer Meeresuntersuchungen, 39, 273, 1985.

Aubinet, Marc and Grelle, Achim and Ibrom, Andreas and Rannik, Üllar and Moncrieff, John and Foken, Thomas and Kowalski, Andy S and Martin, Philippe H and Berbigier, Paul and Bernhofer, Ch and others: Estimates of the annual net carbon and water exchange of forests: the EUROFLUX methodology, in: Advances in ecological research, vol. 30, pp. 113–175, Elsevier, 1999.

Baldocchi, D. D., Hincks, B. B., and Meyers, T. P.: Measuring biosphere-atmosphere exchanges of biologically related gases with micrometeorological methods, Ecology, 69, 1331–1340, 1988.

Barnett, A., Méléder, V., Blommaert, L., Lepetit, B., Gaudin, P., Vyverman, W., Sabbe, K., Dupuy, C., and Lavaud, J.: Growth form defines physiological photoprotective capacity in intertidal benthic diatoms, The ISME journal, 9, 32, 2015.

Barranguet, C., Kromkamp, J., and Peene, J.: Factors controlling primary production and photosynthetic characteristics of intertidal microphytobenthos, Marine Ecology Progress Series, 173, 117–126, 1998.

Benyoucef, I., Blandin, E., Lerouxel, A., Jesus, B., Rosa, P., Méléder, V., Launeau, P., and Barillé, L.: Microphytobenthos interannual variations in a north-European estuary (Loire estuary, France) detected by visible-infrared multispectral remote sensing, Estuarine, Coastal and Shelf Science, 136, 43–52, 2014.

Berg, P., Røy, H., Janssen, F., Meyer, V., Jørgensen, B. B., Huettel, M., and de Beer, D.: Oxygen uptake by aquatic sediments measured with a novel non-invasive eddy-correlation technique, Marine Ecology Progress Series, 261, 75–83, 2003.

Blanchard, G. F. and Cariou-Le Gall, V.: Photo synthetic characteristics of microphytobenthos in Marennes-Oléron Bay, France: Preliminary results, Journal of experimental marine biology and ecology, 182, 1–14, 1994.

Blanchard, G. F., Guarini, J. ., Richard, P., Gros, P., and Mornet, F.: Quantifying the short-term temperature effect on light- saturated photosynthesis of intertidal microphytobenthos, Marine Ecology Progress Series, 134, 309–313, 1996.

Blanchard, G. F., Guarini, J.-M., Gros, P., and Richard, P.: Seasonal effect on the relationship between the photosynthetic capacity of intertidal microphytobenthos and temperature, Journal of Phycology, 33, 723–728, https://doi.org/10.1111/j.0022-3646.1997.00723.x, 1997.

Blanchard, G. F., Guarini, J.-M., Provot, L., Richard, P., and Sauriau, P.-G.: Measurement of ingestion rate of Hydrobia ulvae (Pennant) on intertidal epipelic microalgae: the effect of mud snail density, Journal of Experimental Marine Biology and Ecology, 255, 247–260, 2000.

Blanchard, G. F., Guarini, J.-M., Dang, C., and Richard, P.: Characterizing and quantifying photoinhibition in intertidal microphytobenthos, Journal of phycology, 40, 692–696, 2004.

Bocher, P., Piersma, T., Dekinga, A., Kraan, C., Yates, M. G., Guyot, T., Folmer, E. O., and Radenac, G.: Site-and species-specific distribution patterns of molluscs at five intertidal soft-sediment areas in northwest Europe during a single winter, Marine Biology, 151, 577–594, 2007.

Brito, A. C., Benyoucef, I., Jesus, B., Brotas, V., Gernez, P., Mendes, C. R., Launeau, P., Dias, M. P., and Barillé, L.: Seasonality of microphytobenthos revealed by remote-sensing in a South European estuary, Continental Shelf Research, 66, 83–91, 2013.

Britton, C. and Dodd, J.: Relationships of photosynthetically active radiation and shortwave irradiance, Agricultural Meteorology, 17, 1–7, 1976.

Brock, T. D.: Calculating solar radiation for ecological studies, Ecological Modelling, 14, 1–19, 1981.

Brunet, C., Johnsen, G., Lavaud, J., and Roy, S.: Pigments and photoacclimation processes, 2011.

Cadée, G. and Hegeman, J.: Primary production of the benthic microflora living on tidal flats in the dutch wadden sea, Netherlands Journal of Sea Research, 8, 260–291, https://doi.org/10.1016/0077-7579(74)90020-9, 1974.

Cadée, G. and Hegeman, J.: Distribution of primary production of the benthic microflora and accumulation of organic matter on a tidal flat area, Balgzand, Dutch Wadden Sea, Netherlands Journal of Sea Research, 11, 24–41, 1977.

Cariou-Le Gall, V. and Blanchard, G. F.: Monthly HPLC measurements of pigment concentration from an intertidal muddy sediment of Marennes-Oleron Bay, France, Marine Ecology Progress Series, 121, 171–180, 1995.

Cartaxana, P., Ruivo, M., Hubas, C., Davidson, I., Serôdio, J., and Jesus, B.: Physiological versus behavioral photoprotection in intertidal epipelic and epipsammic benthic diatom communities, Journal of experimental marine biology and ecology, 405, 120–127, 2011.

Cartaxana, P., Vieira, S., Ribeiro, L., Rocha, R. J., Cruz, S., Calado, R., and da Silva, J. M.: Effects of elevated temperature and CO 2 on intertidal microphytobenthos, BMC ecology, 15, 10, 2015.

Cloern, J. E.: Turbidity as a control on phytoplankton biomass and productivity in estuaries, Continental shelf research, pp. 1367–1381, 1987.

Cloern, J. E., Grenz, C., and Vidergar-Lucas, L.: An empirical model of the phytoplankton chlorophyll: carbon ratio-the conversion factor between productivity and growth rate, Limnology and Oceanography, 40, 1313–1321, 1995.

Coelho, H., Vieira, S., and Serôdio, J.: Effects of desiccation on the photosynthetic activity of intertidal microphytobenthos biofilms as studied by optical methods, Journal of Experimental Marine Biology and Ecology, 381, 98–104, 2009.

Coelho, H., Cartaxana, P., Brotas, V., Queiroga, H., and Serôdio, J.: Pheophorbide a in Hydrobia ulvae faecal pellets as a measure of microphytobenthos ingestion: Variation over season and period of day, Aquatic Biology, 13, 119–126, 2011.

Cohn, S. A., Farrell, J. F., Munro, J. D., Ragland, R. L., Weitzell Jr, R. E., and Wibisono, B. L.: The effect of temperature and mixed species composition on diatom motility and adhesion, Diatom Research, 18, 225–243, 2003.

Daggers, T. D., Kromkamp, J. C., Herman, P. M., and Van Der Wal, D.: A model to assess microphytobenthic primary production in tidal systems using satellite remote sensing, Remote sensing of environment, 211, 129–145, 2018.

De Jong, D. and de Jonge, V. N.: Dynamics and distribution of microphytobenthic chlorophyll-a in the Western Scheldt estuary (SW Netherlands), Hydrobiologia, 311, 21–30, 1995.

de Jonge, V. N.: Fluctuations in the organic carbon to chlorophyll a ratios for estuarine benthic diatom populations, Marine Ecology Progress Series, pp. 345–353, 1980.

de Jonge, V. N. and van Beusekom, J. E. E.: Contribution of resuspended microphytobenthos to total phytoplankton in the EMS estuary and its possible role for grazers, Netherlands Journal of Sea Research, 30, 91–105, 1992.

de Jonge, V. N. and van Beusekom, J. E. E.: Wind and tide-induced resuspension of sediment and microphytobenthos from tidal flats in the Ems estuary, Limnology and Oceanography, 40, 776–778, 1995.

de Jonge, V. N., de Boer, W. F., de Jong, D. J., and Brauer, V. S.: Long-term mean annual microphytobenthos chlorophyll a variation correlates with air temperature, Marine Ecology Progress Series, 468, 43–56, 2012.

Demers, S., Therriault, J.-C., Bourget, E., and Bah, A.: Resuspension in the shallow sublittoral zone of a macrotidal estuarine environment: Wind influence, Limnology and Oceanography, 32, 327–339, https://doi.org/10.4319/lo.1987.32.2.0327, 1987.

Dupuy, C., Mallet, C., Guizien, K., Montanié, H., Bréret, M., Mornet, F., Fontaine, C., Nérot, C., and Orvain, F.: Sequential resuspension of biofilm components (viruses, prokaryotes and protists) as measured by erodimetry experiments in the Brouage mudflat (French Atlantic coast), Journal of sea research, 92, 56–65, 2014.

Feuillet-Girard, M., Gouleau, D., Blanchard, G., and Joassard, L.: Nutrient fluxes on an intertidal mudflat in Marennes-Oléron Bay, and influence of the emersion period, Aquatic Living Resources, 10, 49–58, 1997.

García-Robledo, E., Corzo, A., Papaspyrou, S., Jiménez-Arias, J. L., and Villahermosa, D.: Freeze-lysable inorganic nutrients in intertidal sediments: Dependence on microphytobenthos abundance, Marine Ecology Progress Series, 403, 155–163, 2010.

Garcia-Robledo, E., Bohorquez, J., Corzo, A., Jimenez-Arias, J. L., and Papaspyrou, S.: Dynamics of inorganic nutrients in intertidal sediments: Porewater, exchangeable, and intracellular pools, Frontiers in Microbiology, 7, 2016.

Gould, D. M. and Gallagher, E. D.: Field measurement of specific growth rate, biomass, and primary production of benthic diatoms of Savin Hill Cove, Boston, Limnology and Oceanography, 35, 1757–1770, 1990.

Gouleau, D., Jouanneau, J., Weber, O., and Sauriau, P.: Short-and long-term sedimentation on Montportail–Brouage intertidal mudflat, Marennes–Oleron Bay (France), Continental Shelf Research, 20, 1513–1530, 2000.

Guarini, J.-M.: Modélisation de la dynamique du microphytobenthos des vasières intertidales du bassin de Marennes-Oléron. Effets des synchroniseurs physiques sur la régulation de la production, Ph.D. thesis, Paris 6, 1998.

Guarini, J.-M., Blanchard, G. F., Gros, P., and Harrison, S. J.: Modelling the mud surface temperature on intertidal flats to investigate the spatio-temporal dynamics of the benthic microalgal photosynthetic capacity, Marine Ecology Progress Series, 153, 25–36, 1997.

Guarini, J.-M., Blanchard, G., Bacher, C., Gros, P., Riera, P., Richard, P., Gouleau, D., Galois, R., Prou, J., and Sauriau, P.-G.: Dynamics of spatial patterns of microphytobenthic biomass: inferences from a geostatistical analysis of two comprehensive surveys in Marennes-Oléron Bay (France), Marine Ecology Progress Series, pp. 131–141, 1998.

Guarini, J.-M., Blanchard, G., Gros, P., Gouleau, D., and Bacher, C.: Dynamic model of the short-term variability of microphytobenthic biomass on temperate intertidal mudflats, Marine Ecology Progress Series, pp. 291–303, 2000.

Guarini, J.-M., Blanchard, G. F., Gros, P., and Richard, P.: Modelling the dynamics of the microphytobenthic biomass and primary production in European intertidal mudflats , in: Functioning of microphytobenthos in estuaries. Amsterdam, Royal Netherlands Academy of Arts and Sciences, pp. 187–226, Royal Netherlands Academy of Arts and Sciences, 2006.

Guarini, J.-M., Sari, N., and Moritz, C.: Modelling the dynamics of the microalgal biomass in semi-enclosed shallow-water ecosystems, Ecological Modelling, 211, 267–278, 2008.

Hammersley, J. and Handscomb, D.: Monte Carlo Methods, London: Methuen & Co. Ltd, 1964.

Harrison, S. J.: Heat exchanges in muddy intertidal sediments: Chichester Harbour, West Sussex, England, Estuarine, Coastal and Shelf Science, 20, 477–490, 1985.

Harrison, S. J. and Phizacklea, A. P.: Seasonal changes in heat flux and heat storage forth estuary, scotland in the intertidal mudflats of the forth estuary, scotland, Journal of Climatology, 5, 473–485, 1985.

Harrison, S. J. and Phizacklea, A. P.: Vertical temperature gradients in muddy intertidal sediments in the Forth estuary, Scotland, Limnology and Oceanography, 32, 954–963, 1987.

Haubois, A.-G., Guarini, J.-M., Richard, P., Blanchard, G., and Sauriau, P.-G.: Spatio–temporal differentiation in the population structure of Hydrobia ulvae on an intertidal mudflat (Marennes-Oléron Bay, France), Journal of the Marine Biological Association of the United Kingdom, 82, 605–614, 2002.

Haubois, A.-G., Guarini, J.-M., Richard, P., Fichet, D., Radenac, G., and Blanchard, G.: Ingestion rate of the deposit-feeder Hydrobia ulvae (Gastropoda) on epipelic diatoms: effect of cell size and algal biomass, Journal of Experimental Marine Biology and Ecology, 317, 1–12, 2005.

Heilskov, A. C., Alperin, M., and Holmer, M.: Benthic fauna bio-irrigation effects on nutrient regeneration in fish farm sediments, Journal of Experimental Marine Biology and Ecology, 339, 204–225, 2006.

Herlory, O., Guarini, J.-M., Richard, P., and Blanchard, G. F.: Microstructure of microphytobenthic biofilm and its spatio-temporal dynamics in an intertidal mudflat (Aiguillon Bay, France), Marine Ecology Progress Series, 282, 33–44, 2004.

Herman, P. M. J., Middelburg, J. J., Widdows, J., Lucas, C. H., and Heip, C. H. R.: Stable isotopes as trophic tracers: Combining field sampling and manipulative labelling of food resources for macrobenthos, Marine Ecology Progress Series, 204, 79–92, 2000.

Hopkinson, C. and Smith, E. M.: Estuarine respiration: an overview of benthic, pelagic, and whole system respiration, Respiration in aquatic ecosystems, pp. 122–146, 2005.

Hubas, C., Davoult, D., Cariou, T., and Artigas, L. F.: Factors controlling benthic metabolism during low tide along a granulometric gradient in an intertidal bay (Roscoff Aber Bay, France), Marine Ecology Progress Series, 316, 53–68, 2006.

Jansson, B.-O. and Wulff, F.: Ecosystem analysis of a shallow sound in the northern Baltic: a joint study by the Askö group, University of Stockholm, Sweden, 1977.

Jardine, C. B., Bond, A. L., Davidson, P. J., Butler, R. W., and Kuwae, T.: Biofilm consumption and variable diet composition of Western Sandpipers (Calidris mauri) during migratory stopover, PloS one, 10, e0124 164, 2015.

Juneau, P., Barnett, A., Méléder, V., Dupuy, C., and Lavaud, J.: Combined effect of high light and high salinity on the regulation of photosynthesis in three diatom species belonging to the main growth forms of intertidal flat inhabiting microphytobenthos, Journal of experimental marine biology and ecology, 463, 95–104, 2015.

Kang, C., Lee, Y., Eun, J. C., Shin, J., Seo, I., and Hong, J.: Microphytobenthos seasonality determines growth and reproduction in intertidal bivalves, Marine Ecology Progress Series, 315, 113–127, 2006.

Kofoed, L. H.: The feeding biology of Hydrobia ventrosa (Montagu). II. Allocation of the components of the carbon-budget and the significance of the secretion of dissolved organic material, Journal of Experimental Marine Biology and Ecology, 19, 243–256, 1975.

Kromkamp, J., Barranguet, C., and Peene, J.: Determination of microphytobenthos PSII quantum efficiency and photosynthetic activity by means of variable chlorophyll fluorescence, Marine Ecology Progress Series, 162, 45–55, 1998.

Krumme, U., Keuthen, H., Barletta, M., Saint-Paul, U., and Villwock, W.: Resuspended intertidal microphytobenthos as major diet component of planktivorous Atlantic anchoveta Cetengraulis edentulus (Engraulidae) from equatorial mangrove creeks, Ecotropica, 14, 121–128, 2008.

Kwon, B.-O., Koh, C.-H., Khim, J. S., Park, J., Kang, S.-G., and Hwang, J. H.: The relationship between primary production of microphytobenthos and tidal cycle on the Hwaseong mudflat, west coast of Korea, Journal of Coastal Research, 30, 1188–1196, 2014.

Laverock, B., Gilbert, J. A., Tait, K., Osborn, A. M., and Widdicombe, S.: Bioturbation: impact on the marine nitrogen cycle, 2011.

Laviale, M., Barnett, A., Ezequiel, J., Lepetit, B., Frankenbach, S., Méléder, V., Serôdio, J., and Lavaud, J.: Response of intertidal benthic microalgal biofilms to a coupled light–temperature stress: evidence for latitudinal adaptation along the Atlantic coast of Southern Europe, Environmental microbiology, 17, 3662–3677, 2015.

Le Fouest, V., Zakardjian, B., Xie, H., Raimbault, P., Joux, F., and Babin, M.: Modeling plankton ecosystem functioning and nitrogen fluxes in the oligotrophic waters of the Beaufort Sea, Arctic Ocean: a focus on light-driven processes, Biogeosciences, 10, 4785–4800, 2013.

Light, B. R. and Beardall, J.: Photosynthetic characteristics of sub-tidal benthic microalgal populations from a temperate, shallow water marine ecosystem, Aquatic Botany, 70, 9–27, 2001.

Losordo, T. M. and Piedrahita, R. H.: Modelling temperature variation and thermal stratification in shallow aquaculture ponds, Ecological modelling, 54, 189–226, 1991.

Lucas, C. H., Banham, C., and Holligan, P. M.: Benthic-pelagic exchange of microalgae at a tidal flat. 2. Taxonomic analysis, Marine Ecology Progress Series, 212, 39–52, 2001.

MacIntyre, H. L., Kana, T. M., Anning, T., and Geider, R. J.: Photoacclimation of photosynthesis irradiance response curves and photosynthetic pigments in microalgae and cyanobacteria, Journal of phycology, 38, 17–38, 2002.

Mann, K.: The Ecology of coastal waters—A systems approach, Blackwell, Oxford, 1982.

Mariotti, G. and Fagherazzi, S.: Modeling the effect of tides and waves on benthic biofilms, Journal of Geophysical Research: Biogeosciences, 117, 2012.

Méléder, V., Launeau, P., Barillé, L., and Rincé, Y.: Cartographie des peuplements du microphytobenthos par télédétection spatiale visible-infrarouge dans un écosystème conchylicole, Comptes Rendus Biologies, 326, 377–389, 2003.

Méléder, V., Jesus, B., Barnett, A., Barillé, L., and Lavaud, J.: Microphytobenthos primary production estimated by hyperspectral reflectance, PloS one, p. e0197093, 2018.

Montagna, P. A., Blanchard, G. F., and Dinet, A.: Effect of production and biomass of intertidal microphytobenthos on meiofaunal grazing rates, Journal of Experimental Marine Biology and Ecology, 185, 149–165, https://doi.org/10.1016/0022-0981(94)00138-4, http://www.sciencedirect.com/science/article/pii/0022098194001384, 1995.

Morris, E. P. and Kromkamp, J. C.: Influence of temperature on the relationship between oxygen-and fluorescence-based estimates of photosynthetic parameters in a marine benthic diatom (Cylindrotheca closterium), European Journal of Phycology, 38, 133–142, 2003.

Nishiyama, Y., Allakhverdiev, S. I., and Murata, N.: A new paradigm for the action of reactive oxygen species in the photoinhibition of photosystem II, Biochimica et Biophysica Acta (BBA)-Bioenergetics, 1757, 742–749, 2006.

Orvain, F., Sauriau, P.-G., Sygut, A., Joassard, L., and Le Hir, P.: Interacting effects of Hydrobia ulvae bioturbation and microphytobenthos on the erodibility of mudflat sediments, Marine ecology progress series, 278, 205–223, 2004.

Orvain, F., De Crignis, M., Guizien, K., Lefebvre, S., Mallet, C., Takahashi, E., and Dupuy, C.: Tidal and seasonal effects on the short-term temporal patterns of bacteria, microphytobenthos and exopolymers in natural intertidal biofilms (Brouage, France), Journal of Sea Research, 92, 6–18, 2014.

Pascal, P.-Y., Dupuy, C., Richard, P., Haubois, A.-G., and Niquil, N.: Influence of environment factors on bacterial ingestion rate of the deposit-feeder Hydrobia ulvae and comparison with meiofauna, Journal of Sea Research, 60, 151–156, 2008.

Pascal, P.-Y., Dupuy, C., Richard, P., Mallet, C., Niquilb, N., et al.: Seasonal variation in consumption of benthic bacteria by meio-and macrofauna in an intertidal mudflat, Limnology and Oceanography, 54, 1048–1059, 2009.

Pascual, E. and Drake, P.: Physiological and behavioral responses of the mud snails Hydrobia glyca and Hydrobia ulvae to extreme water temperatures and salinities: implications for their spatial distribution within a system of temperate lagoons, Physiological and Biochemical Zoology, 81, 594–604, 2008.

Perissinotto, R., Nozais, C., Kibirige, I., and Anandraj, A.: Planktonic food webs and benthic-pelagic coupling in three South African temporarily-open estuaries, Acta Oecologica, 24, S307–S316, https://doi.org/10.1016/S1146-609X(03)00028-6, proceedings of the Plankton Symposium, Espinho, Portugal, 2003.

Perkins, R. G., Underwood, G. J. C., Brotas, V., Snow, G. C., Jesus, B., and Ribeiro, L.: Responses of microphytobenthos to light: Primary production and carbohydrate allocation over an emersion period, Marine Ecology Progress Series, 223, 101–112, 2001.

Piccolo, M., Perillo, G., and Daborn, G.: Soil temperature variations on a tidal flat in Minas Basin, Bay of Fundy, Canada, Estuarine, Coastal and Shelf Science, 36, 345–357, 1993.

Pinckney, J. L., Carman, K. R., Lumsden, S. E., and Hymel, S. N.: Microalgal-meiofaunal trophic relationships in muddy intertidal estuarine sediments, Aquatic Microbial Ecology, 31, 99–108, 2003.

Platt, T. and Jassby, A. D.: The relationship between photosynthesis and light for natural assemblages of coastal marine phytoplankton, Journal of Phycology, 12, 421–430, 1976.

Pniewski, F. F., Biskup, P., Bubak, I., Richard, P., Latała, A., and Blanchard, G.: Photo-regulation in microphytobenthos from intertidal mudflats and non-tidal coastal shallows, Estuarine, Coastal and Shelf Science, 152, 2015.

Polsenaere, P., Lamaud, E., Lafon, V., Bonnefond, J.-M., Bretel, P., Delille, B., Deborde, J., Loustau, D., and Abril, G.: Spatial and temporal CO2 exchanges measured by Eddy Covariance over a temperate intertidal flat and their relationships to net ecosystem production, Biogeosciences, pp. 249–268, 2012.

Pond, S., Fissel, D., and Paulson, C.: A note on bulk aerodynamic coefficients for sensible heat and moisture fluxes, Boundary-Layer Meteorology, 6, 333–339, 1974.

Rakotomalala, C., Guizien, K., Grangeré, K., Lefebvre, S., Dupuy, C., and Orvain, F.: Modelling the functioning of a coupled Microphytobentic-EPS-bacterial system in intertidal mudflats , submitted.

Remmert, H.: Ökologie: ein Lehrbuch, Springer-Verlag, 2013.

Rijstenbil, J.: Effects of UVB radiation and salt stress on growth, pigments and antioxidative defence of the marine diatom Cylindrotheca closterium, Marine Ecology Progress Series, 254, 37–47, 2003.

Roncarati, F., Rijstenbil, J., and Pistocchi, R.: Photosynthetic performance, oxidative damage and antioxidants in Cylindrotheca closterium in response to high irradiance, UVB radiation and salinity, Marine biology, 153, 965–973, 2008.

Round, F.: Benthic marine diatoms, Oceanogr. Mar. Biol. Ann. Rev., 9, 83–139, 1971.

Sahan, E., Sabbe, K., Creach, V., Hernandez-Raquet, G., Vyverman, W., Stal, L. J., and Muyzer, G.: Community structure and seasonal dynamics of diatom biofilms and associated grazers in intertidal mudflats, Aquatic Microbial Ecology, 47, 253–266, 2007.

Saint-Béat, B., Dupuy, C., Agogué, H., Carpentier, A., Chalumeau, J., Como, S., David, V., De Crignis, M., Duchêne, J.-C., Fontaine, C., et al.: How does the resuspension of the biofilm alter the functioning of the benthos–pelagos coupled food web of a bare mudflat in Marennes-Oléron Bay (NE Atlantic)?, Journal of Sea Research, 92, 144–157, 2014.

Sakshaug, E., Bricaud, A., Dandonneau, Y., Falkowski, P. G., Kiefer, D. A., Legendre, L., Morel, A., Parslow, J., and Takahashi, M.: Parameters of photosynthesis: definitions, theory and interpretation of results, Journal of Plankton Research, 19, 1637–1670, 1997.

Santos, C. D., Granadeiro, J. P., and Palmeirim, J. M.: Feeding ecology of dunlin Calidris alpina in a southern European estuary, Ardeola, 52, 235–252, 2005.

Sauer, J., Wenderoth, K., Maier, U. G., and Rhiel, E.: Effects of salinity, light and time on the vertical migration of diatom assemblages, Diatom Research, 17, 189–203, dedicated to Prof. Dr. WE Krumbein on the occasion of his 65th birthday, 2002.

Sauriau, P.-G., Mouret, V., and Rince, J.-P.: Trophic system of wild soft-bottom molluscs in the Marennes-Oleron oyster-farming bay, Oceanologica Acta, 12, 193–204, 1989.

Scholz, B. and Liebezeit, G.: Growth responses of 25 benthic marine Wadden Sea diatoms isolated from the Solthörn tidal flat (southern North Sea) in relation to varying culture conditions, Diatom Research, 27, 65–73, 2012.

Serodio, J. and Catarino, F.: Fortnightly light and temperature variability in estuarine intertidal sediments and implications for microphytobenthos primary productivity, Aquatic Ecology, pp. 235–241, 1999.

Sibert, V., Zakardjian, B., Saucier, F., Gosselin, M., Starr, M., and Senneville, S.: Spatial and temporal variability of ice algal production in a 3D ice–ocean model of the Hudson Bay, Hudson Strait and Foxe Basin system, Polar Research, 29, 353–378, 2010.

Sibert, V., Zakardjian, B., Gosselin, M., Starr, M., Senneville, S., and LeClainche, Y.: 3D bio-physical model of the sympagic and planktonic productions in the Hudson Bay System, Journal of Marine Systems, 88, 401–422, 2011.

Struski, C. and Bacher, C.: Preliminary estimate of primary production by phytoplankton in Marennes-Oléron Bay, France, Estuarine, Coastal and Shelf Science, pp. 323–334, 2006.

Talling, J.: The phytoplankton population as a compound photosynthetic system, New phytologist, 56, 133–149, 1957.

Thompson, R., Roberts, M., Norton, T., and Hawkins, S.: Feast or famine for intertidal grazing molluscs: a mis-match between seasonal variations in grazing intensity and the abundance of microbial resources, Hydrobiologia, 440, 357–367, 2000.

Tucker, C. J.: Red and photographic infrared linear combinations for monitoring vegetation, Remote sensing of Environment, 8, 127–150, 1979.

Ubertini, M., Lefebvre, S., Gangnery, A., Grangeré, K., Le Gendre, R., and Orvain, F.: Spatial variability of benthic-pelagic coupling in an estuary ecosystem: consequences for microphytobenthos resuspension phenomenon, PloS one, 7, e44 155, 2012.

Underwood, G.: Microphytobenthos, in: Encyclopedia of Ocean Sciences, edited by Steele, J. H., pp. 1770–1777, Academic Press, Oxford, 2001.

Underwood, G. and Kromkamp, J.: Primary Production by Phytoplankton and Microphytobenthos in Estuaries, in: Estuaries, edited by Nedwell, D. and Raffaelli, D., vol. 29 of *Advances in Ecological Research*, pp. 93–153, Academic Press, https://doi.org/10.1016/S0065-2504(08)60192-0, 1999.

Underwood, G. and Smith, D.: Predicting epipelic diatom exopolymer concentrations in intertidal sediments from sediment chlorophyll a, Microbial Ecology, 35, 116–125, 1998.

Underwood, G. J. C.: Seasonal and spatial variation in epipelic diatom assemblages in the severn estuary, Diatom Research, 9, 451–472, 1994.

Van Bavel, C. and Hillel, D.: Calculating potential and actual evaporation from a bare soil surface by simulation of concurrent flow of water and heat, Agricultural Meteorology, 17, 453–476, 1976.

Vieira, S., Cartaxana, P., Máguas, C., and Marques Da Silva, J.: Photosynthesis in estuarine intertidal microphytobenthos is limited by inorganic carbon availability, Photosynthesis Research, 128, 85–92, 2016.

Weerman, E. J., Herman, P. M., and Van de Koppel, J.: Top-down control inhibits spatial self-organization of a patterned landscape, Ecology, 92, 487–495, 2011.

Yamaguchi, A., Umezawa, Y., Wada, M., and Sayama, M.: Potential contribution of microalgal intracellular phosphorus to phosphorus distribution in tidal flat sediments during winter, Plankton and Benthos Research, 10, 1–10, 2015.

Zemmelink, H., Slagter, H., Van Slooten, C., Snoek, J., Heusinkveld, B., Elbers, J., Bink, N., Klaassen, W., Philippart, C., and De Baar, H.: Primary production and eddy correlation measurements of CO2 exchange over an intertidal estuary, Geophysical research letters, 2009.

Biogeosciences Discuss., https://doi.org/10.5194/bg-2018-325
Manuscript under review for journal Biogeosciences
Discussion started: 10 July 2018

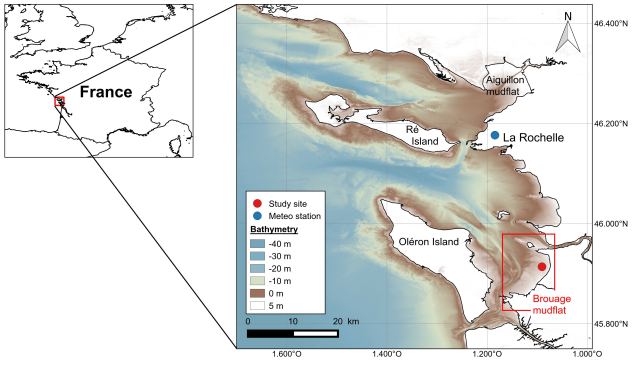

Figure 1. Bathymetric map of the Pertuis Charentais (source: French marine service for hydrography and oceanography (SHOM)) and location of the main intertidal mudflats. The study site is represented by a red full point and the Meteo France weather station is represented by a blue full point.

Biogeosciences Discuss., https://doi.org/10.5194/bg-2018-325
Manuscript under review for journal Biogeosciences
Discussion started: 10 July 2018

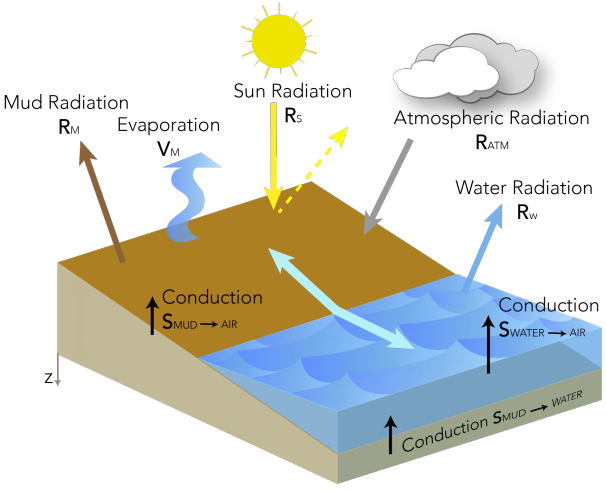

Figure 2. Conceptual scheme of heat exchange at the mud surface in the intertidal zone. Fluxes contributing to heat energy balance are represented by arrows during emersion and immersion periods. Modified from Guarini et al. (1997).

Biogeosciences Discuss., https://doi.org/10.5194/bg-2018-325
Manuscript under review for journal Biogeosciences
Discussion started: 10 July 2018

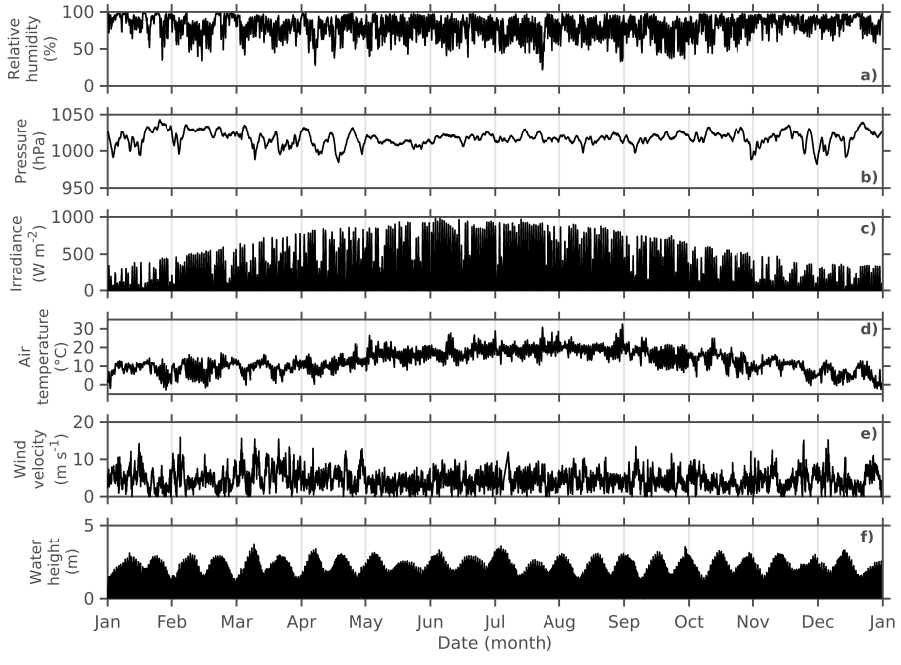

Figure 3. Annual cycle of forcings in 2008. a) Relative humidity. b) Atmospheric pressure above the sea. c) Global irradiance. d) Air temperature in the shade. e) Wind velocity. f) Water height at the study site. Meteorological data comes from the weather station located near the airport of La Rochelle and the water height was measured at the tide gauge of La Rochelle-La Pallice corrected by the bathymetry of the study site.

Biogeosciences Discuss., https://doi.org/10.5194/bg-2018-325
Manuscript under review for journal Biogeosciences
Discussion started: 10 July 2018

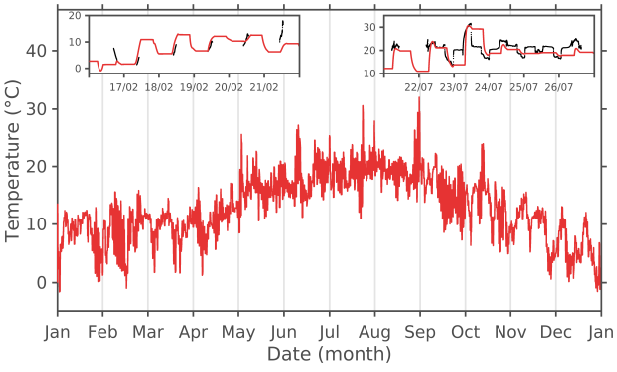

Figure 4. Observed (black points) and simulated (red lines) mud surface temperature in 2008.

Biogeosciences Discuss., https://doi.org/10.5194/bg-2018-325
Manuscript under review for journal Biogeosciences
Discussion started: 10 July 2018

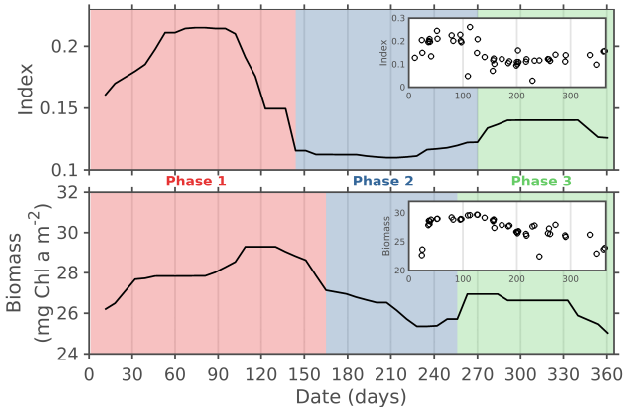

Figure 5. Normalized difference vegetation index and simulated biofilm daily maximum biomass in 2008. Original data (small plots) have been regularized and filtered with running medians (window size = 7). NDVI is calculated at the pixel corresponding to the study site. Phases are determined according the amplitude of the sign change of the second order derivative.

Biogeosciences Discuss., https://doi.org/10.5194/bg-2018-325
Manuscript under review for journal Biogeosciences
Discussion started: 10 July 2018

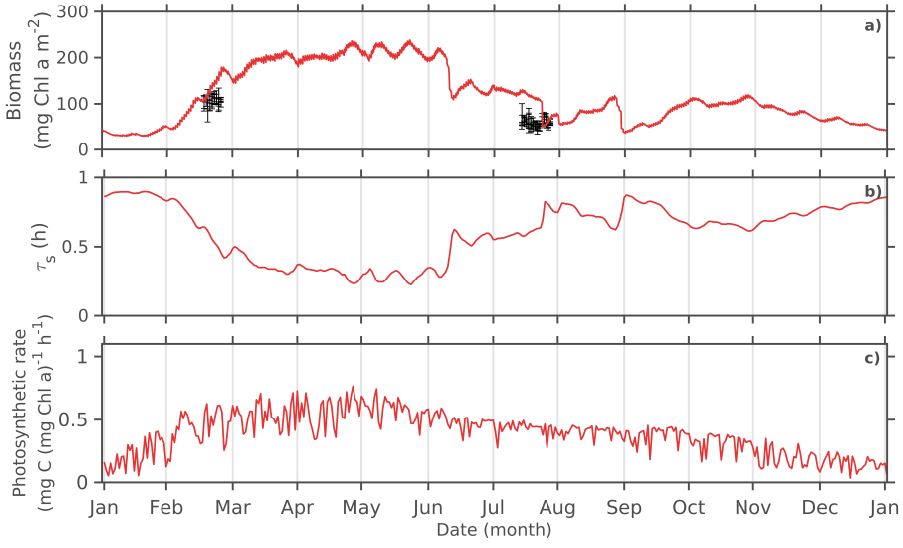

Figure 6. Seasonal cycle of the 2008: **a)** simulated total MPB biomass; **b)** average time spent by a unit of MPB biomass at the sediment surface; **c)** average mass-specific photosynthetic rate during daytime low tides. Black error bars correspond to observations (± sd).

Biogeosciences Discuss., https://doi.org/10.5194/bg-2018-325
Manuscript under review for journal Biogeosciences
Discussion started: 10 July 2018

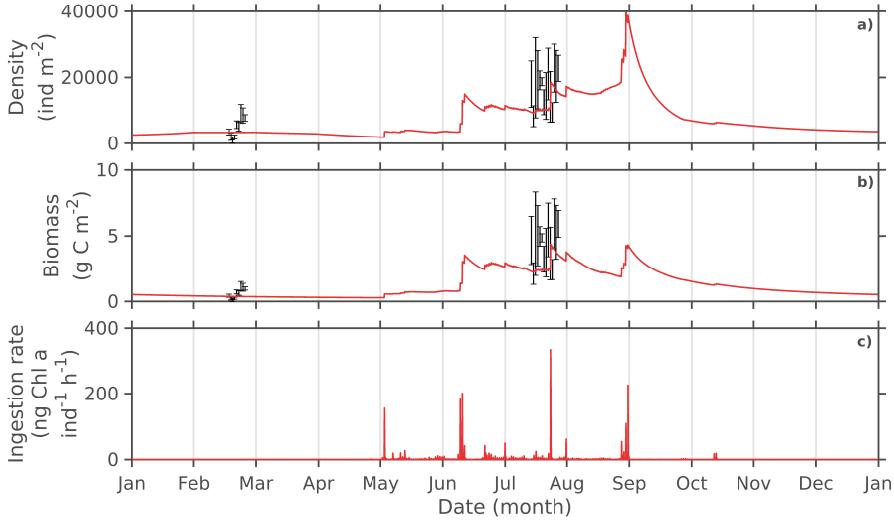

Figure 7. Seasonal cycle of the 2008: **a)** Simulated *P. ulvae* density; **b)** simulated biomass of *P. ulvae*; **c)** individual ingestion rate by *P. ulvae*. Black error bars correspond to observations (± sd).

Biogeosciences Discuss., https://doi.org/10.5194/bg-2018-325
Manuscript under review for journal Biogeosciences
Discussion started: 10 July 2018

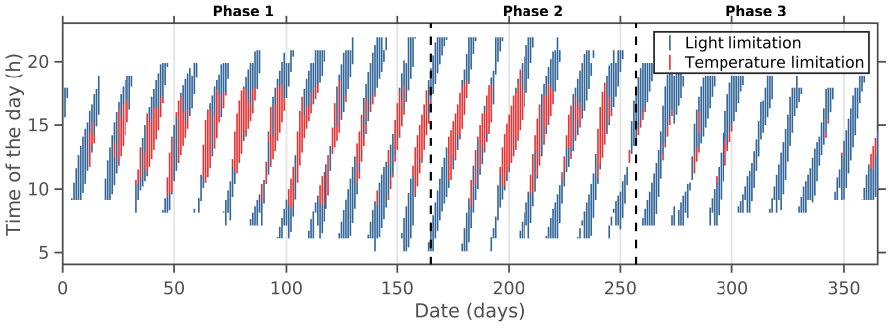

Figure 8. Seasonal cycle of daily hours of limitation by light and temperature over daytime emersion periods in 2008.

Biogeosciences Discuss., https://doi.org/10.5194/bg-2018-325
Manuscript under review for journal Biogeosciences
Discussion started: 10 July 2018

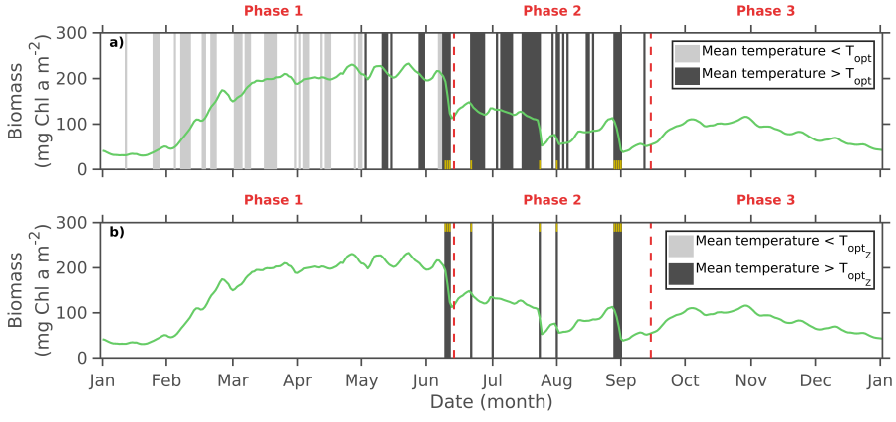

Figure 9. Seasonal cycle of the MPB biomass (green full line) along with the daily limiting driver in terms of duration for temperature and in terms of biomass produced vs. ingestion by grazing in 2008: a) Days dominated by temperature limitation, b) days dominated by grazing pressure. Temperature conditions are averaged over the daytime emersion period. The yellow bars indicate the match between temperature and grazing -limited days.

Biogeosciences Discuss., https://doi.org/10.5194/bg-2018-325
Manuscript under review for journal Biogeosciences
Discussion started: 10 July 2018

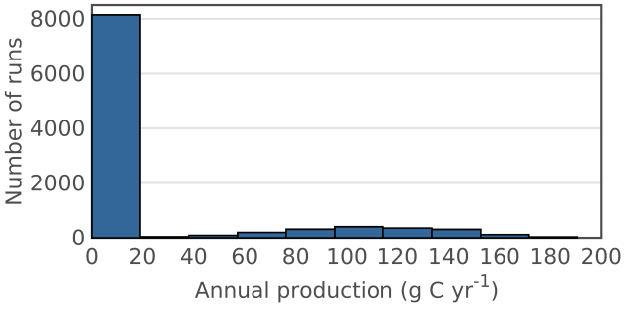

Figure 10. Sensitivity analysis of the simulated annual MPB PP.

Biogeosciences Discuss., https://doi.org/10.5194/bg-2018-325
Manuscript under review for journal Biogeosciences
Discussion started: 10 July 2018

Table 1. Conceptual schemes and differential equations of the biological model including the MPB biomass within the sediment 1st cm (F), the MPB biomass within the biofilm (S) and the biomass of *P. ulvae* (Z). The upper case corresponds to daytime emersion periods, when MPB cells migrate at the sediment surface (①) to produce and transfer biomass to the sediment 1st cm (②). The middle case corresponds to day or night time emersion period when MPB cells migrate down to the sediment 1st cm (③). The lower case corresponds to immersion periods, when MPB cells are chronically resuspended from the 1st cm to the water column (④) and the remaining MPB cells within the biofilm finish their downward migration (③). *P. ulvae* grazing is only active during emersion periods (righ side up on schemes)(modified from Guarini et al., 2008).

Scheme	Cases	Equations
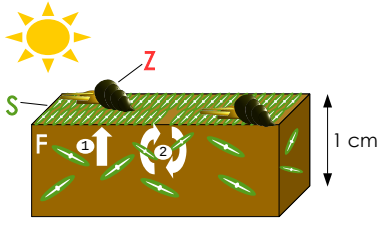	Day Low tide $\tau > 0$	$\frac{dS}{dt} = \left(r_F F + P^b S\right)\left(1 - \frac{S}{S_{max}}\right) - m_S S$ $-min\left[IR\left(\frac{Z}{W_Z^{mean}}\right), S_{IR}\right] \times H\left(F, F_{mini}\right)$ $\frac{dF}{dt} = -r_F F\left(1 - \frac{S}{S_{max}}\right) + P^b S\left(\frac{S}{S_{max}}\right) - m_F F$ $\frac{dZ}{dt} = \gamma \times min\left[IR\left(\frac{Z}{W_Z^{mean}}\right), S_{IR}\right] \times H\left(F, F_{mini}\right) - m_Z Z$ $\frac{d\tau}{dt} = -1$
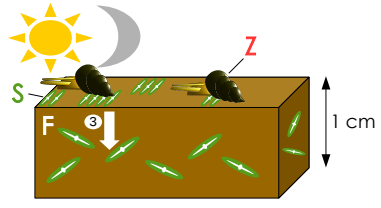	Day Low tide $\tau \leq 0$	$\frac{dS}{dt} = -r_S S - m_S S - min\left[IR\left(\frac{Z}{W_Z^{mean}}\right), S_{IR}\right] \times H\left(F, F_{mini}\right)$ $\frac{dF}{dt} = r_S S - m_F F$ $\frac{dZ}{dt} = \gamma \times min\left[IR\left(\frac{Z}{W_Z^{mean}}\right), S_{IR}\right] \times H\left(F, F_{mini}\right) - m_Z Z$ $\frac{d\tau}{dt} = -1$
	Night Low tide	$\frac{dS}{dt} = -r_S S - m_S S - min\left[IR\left(\frac{Z}{W_Z^{mean}}\right), S_{IR}\right] \times H\left(F, F_{mini}\right)$ $\frac{dF}{dt} = r_S S - m_F F$ $\frac{dZ}{dt} = \gamma \times min\left[IR\left(\frac{Z}{W_Z^{mean}}\right), S_{IR}\right] \times H\left(F, F_{mini}\right) - m_Z Z$ $\tau = \left(\frac{F}{S_{max}} + 1\right) \times \tau_s$
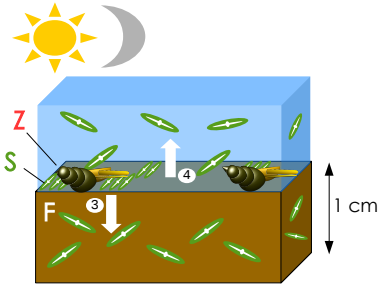	High tide	$\frac{dS}{dt} = -r_S S - m_S S$ $\frac{dF}{dt} = r_S S - \nu_F F$ $\frac{dZ}{dt} = -m_Z Z$ $\tau = \left(\frac{F}{S_{max}} + 1\right) \times \tau_s$

Biogeosciences Discuss., https://doi.org/10.5194/bg-2018-325
Manuscript under review for journal Biogeosciences
Discussion started: 10 July 2018

Table 2. Contribution of light and temperature limitation during the three phases of the MPB seasonal cycle.

Phase	Temperature	Light
Phase 1	33.3 %	66.7 %
Phase 2	39.5 %	60.5 %
Phase 3	0 %	100 %

Biogeosciences Discuss., https://doi.org/10.5194/bg-2018-325
Manuscript under review for journal Biogeosciences
Discussion started: 10 July 2018

Table 3. Ranges of values for the random selection of parameters value used in the Monte-Carlo sensitivity analysis

Parameter	Unit	Range	Reference
T_{opt} (temperature optimum for photosynthesis)	°C	[15; 40]	Blanchard et al. (1997); Hubas et al. (2006); Morris and Kromkamp (2003); Rakotomalala et al. (submitted)
T_{max} (temperature maximum for photosynthesis)	°C	[T_{opt}+1; 40]	Same as T_{opt}
E_k (light saturation parameter)	$\mathrm{W\,m^{-2}}$	[2.5; 180]	Blanchard and Cariou-Le Gall (1994); Barranguet et al. (1998); Light and Beardall (2001); Pniewski et al. (2015); Barnett et al. (2015) and references within
K_E (half-saturation constant for light use)	$\mathrm{Ein\,m^{-2}\,d^{-1}}$	[1; 20]	Sibert et al. (2011); Le Fouest et al. (2013)
T_{opt_Z} (optimal temperature for grazing)	°C	[15; 30]	Pascual and Drake (2008)
α_Z (shape parameter of the temperature related grazing)	-	[0; 0.8]	Present study

Biogeosciences Discuss., https://doi.org/10.5194/bg-2018-325
Manuscript under review for journal Biogeosciences
Discussion started: 10 July 2018

Table 4. Metrics obtained from the model sensitivity analysis on annual MPB PP.

	Sustainable primary production runs							Vanishing primary production runs						
	T_{opt}	T_{max}	T_{opt_Z}	α_Z	E_k	K_E	T_{amp}	T_{opt}	T_{max}	T_{opt_Z}	α_Z	E_k	K_E	T_{amp}
R	-0.24	0.22	0.16	-0.11	-0.56	-0.015	0.39	-0.35	-0.12	-0.014	0.0071	0.022	-0.041	0.44
Mean	19.00	34.00	22.00	0.39	77.00	12.00	15.00	29.00	34.00	22.00	0.40	95.00	10.00	4.90
σ_{norm}	0.14	0.14	0.19	0.60	0.64	0.43	0.28	0.22	0.16	0.19	0.58	0.54	0.54	0.73
Min	15.00	20.00	15.00	0.00	2.50	1.00	4.50	15.00	16.00	15.00	0.00	2.50	1.00	0.051
Max	27.00	40.00	30.00	0.80	180.00	20.00	25.00	40.00	41.00	30.00	0.80	180.00	20.00	20.00

R is the Pearson's correlation coefficient between annual production values from the different runs with the parameters values associated. T_{amp} corresponds to the difference between T_{max} and T_{opt}. σ_{norm} is the normalized standard deviation i.e. the standard deviation divided by the mean.

Biogeosciences Discuss., https://doi.org/10.5194/bg-2018-325
Manuscript under review for journal Biogeosciences
Discussion started: 10 July 2018

Table 5. Temperature optimum and maximum for photosynthesis (T_{opt} and T_{max}, respectively; °C).

Location	T_{opt}	T_{max}	Reference
Marennes-Oléron (France)	25	38	Blanchard et al. (1997)
Roscoff (France)	21	32.5	Hubas et al. (2006)
Ems Dollard (Netherlands)	30	40	Morris and Kromkamp (2003)
Aiguillon Cove (France)	20	30	Rakotomalala et al. (submitted)
Marennes-Oléron (France)	18	38	Present study

Biogeosciences Discuss., https://doi.org/10.5194/bg-2018-325
Manuscript under review for journal Biogeosciences
Discussion started: 10 July 2018

Table A1. Equations of the processes involved in the sediment temperature model

Process	Symbol meaning
Atmospheric and solar radiation	
$R_{sth} = R_0 sin(h)(1-A)$	R_{sth} : cloudless sky theoritical solar radiation
formulated by Brock (1981)	R_0 : solar constant
	h : sun height
	A : albedo
$R_{Atm} = \varepsilon_A \sigma T_A^4 (\zeta - k)$	ε_A: emissivity of air
	σ: Stephan-Boltzman constant
	T_A : measured air temperature
	ζ: constant ($2 \geq \zeta \geq 1$)
	k: attenuation coefficient
$\varepsilon_A = 0.937 \times 10^{-5} T_A^2$	
$k = \frac{R_S}{R_{sth}}$	R_S: solar radiation
$sin(h) = sin(\delta)sin(\phi) + cos(\delta)cos(\phi)cos(AH)$	δ: declination of the sun
	ϕ: latitude of the area
	AH: true horary angle
Mud radiation	
$R_M = \varepsilon_M \sigma T_M^4 (z_0, t)$	ε_M: emissivity of mud
Conduction	
$S_{Mud \to Air} = \rho_A C_{P_A} C_{h_{M \to A}} (1+U)(T_M(z_0,t) - T_A)$	ρ_A: air volumetric mass
formulated by Pond et al. (1974)	C_{P_A}: specific heat of air at constant pressure
	$C_{h_{M \to A}}$: bulk transfer coefficient for conduction between mud and air
	U: wind speed measured at 10 m
$S_{Air \to Water} = \rho_A C_{P_A} C_{h_{A \to W}} (1+U)(T_W(t) - T_A)$	$C_{h_{A \to W}}$: bulk transfer coefficient for conduction between air and water
Evaporation	
$V_W = \rho_A L_V C_V (1+U)\left[q_S \left(1 - \frac{q_A}{q_S}\right)\right]$	L_V: latent heat evaporation
	C_V: bulk transfer coefficient for evaporation
	q_S: specific humidity of saturated air at water temperature
	q_A: absolute air humidity
$L_V = [2500.84 - 2.35(T_E - 273.15)] \times 10^3$	T_E: temperature of interstitial water (in equilibrium with mud temperature)
formulated by Van Bavel and Hillel (1976)	
$q_S = \frac{\lambda p_{sat}^V}{p_{Atm} - (1-\lambda) p_{sat}^V}$	λ: ratio between mass constant for dry air and mass constant for the vapor
	p_{sat}^V: vapor pressure in saturation at interstitial water temperature
	p_{Atm}: atmospheric pressure
$p_{sat}^V = exp\{2.3\left[\frac{7.5(T_E - 273.15)}{237.3 + (T_E - 273.15)} + 0.76\right]\}$	
Water radiation	
$R_W = \sigma T_W^4 (t)$	

k is imposed to 1 if greater than 1. During night periods, k is an average of the values 2 h before the night.

Biogeosciences Discuss., https://doi.org/10.5194/bg-2018-325
Manuscript under review for journal Biogeosciences
Discussion started: 10 July 2018

Table A2. Parameters in the mud surface temperature model

Parameter	Description	Value	Unit
General equations			
η	Conductivity	0.8	$\mathrm{W\,m^{-1}\,K^{-1}}$
ρ_S	Soil volumetric mass	2650	$\mathrm{kg\,m^{-3}}$
ρ_W	Water volumetric mass	1000	$\mathrm{kg\,m^{-3}}$
ξ	Mud porosity	0.62	%
μ	Thermal diffusivity	0.48×10^{-6}	$\mathrm{m^2\,s^{-1}}$
Solar radiations			
R_0	Solar constant	1353	$\mathrm{W\,m^{-2}}$
A	Albedo	0.08	-
Atmospheric radiations			
σ	Stephan-Boltzman	5.67×10^{-8}	$\mathrm{W\,m^{-2}\,K^{-4}}$
ζ	Constant	Radiation on water : 1.05	-
	Radiation on mud : 1.9	-	
Mud radiation			
ε_M	Mud emissivity	0.96	-
Conduction			
ρ_A	Air volumetric mass	1.2929	$\mathrm{kg\,m^{-3}}$
C_{P_A}	Air specific heat	1003	$\mathrm{J\,kg^{-1}\,K^{-1}}$
C_{P_W}	Water specific heat	4180	$\mathrm{J\,kg^{-1}\,K^{-1}}$
$C_{h_{M\to A}}$	Mud-air bulk coefficient	1	-
$C_{h_{A\to W}}$	Air-water bulk coefficient	0.014	-
Evaporation			
C_V	Bulk coefficient	0.0014	-
λ	Constant ratio	0.621	-

Biogeosciences Discuss., https://doi.org/10.5194/bg-2018-325
Manuscript under review for journal Biogeosciences
Discussion started: 10 July 2018

Table A3. Biological model parameters

Symbol	Description	Value	Unit	Source
MPB				
r_S	Transfer rate of biomass from S to F	10	h^{-1}	Guarini et al. (2008)
r_F	Transfer rate of biomass from F to S	1	h^{-1}	Guarini et al. (2008)
m_S	Loss rate of biomass of S	0.001	h^{-1}	Guarini et al. (2008)
m_F	Loss rate of biomass of F during emersion period	0.001	h^{-1}	Guarini et al. (2008)
ν_F	Loss rate of biomass of F during immersion period	0.0035	h^{-1}	Present study
F_{min}	Minimum biomass of F	25	mg chl a m^{-2}	Present study
F_{max}	Maximum biomass of F	300	mg chl a m^{-2}	Guarini et al. (1998)
S_{max}	Maximum biomass of S	25	mg chl a m^{-2}	Guarini et al. (2000)
$\tau_{s_{min}}$	Minimum time spent by a unit of S_{max} at the surface	0.02	h	Present study
$\tau_{s_{max}}$	Maximum time spent by a unit of S_{max} at the surface	1	h	Blanchard et al. (2004)
E_k	Light saturation parameter	100	$\mathrm{W\,m}^{-2}$	Guarini et al. (2000)
P^b_{MAX}	Maximum photosynthetic capacity in April	11.18	µg C (µg chl a)$^{-1}$ h^{-1}	Blanchard et al. (1997)
	Maximum photosynthetic capacity in June	7.56	µg C (µg chl a)$^{-1}$ h^{-1}	Blanchard et al. (1997)
	Maximum photosynthetic capacity in September	5.81	µg C (µg chl a)$^{-1}$ h^{-1}	Blanchard et al. (1997)
	Maximum photosynthetic capacity in December	3.04	µg C (µg chl a)$^{-1}$ h^{-1}	Blanchard et al. (1997)
T_{opt}	Optimum temperature for photosynthesis	18	°C	Present study
T_{max}	Maximum temperature for photosynthesis	38	°C	Blanchard et al. (1997)
β	Shape parameter of the P-T relationship in April	3.90	-	Blanchard et al. (1997)
	Shape parameter of the P-T relationship in June	2.80	-	Blanchard et al. (1997)
	Shape parameter of the P-T relationship in September	1.76	-	Blanchard et al. (1997)
	Shape parameter of the P-T relationship in December	1.03	-	Blanchard et al. (1997)
K_E	Half-saturation constant for light use	20	Ein m^{-2} d^{-1}	Present study
$\left(\frac{Chla}{C}\right)_{min}$	Minimum Chl a: C ratio	0.0125	g chl a g C $^{-1}$	Present study
Grazer *P. ulvae*				
α_Z	Shape parameter of the temperature related grazing	0.55	-	Present study
T_{opt_Z}	Optimum temperature for grazing	20	°C	Pascual and Drake (2008)
IR_{max}	Maximum individual ingestion rate	385	ng chl a ind^{-1} h^{-1}	Coelho et al. (2011)
m_Z^{min}	Minimum mortality rate of *P. ulvae*	6×10^{-7}	h^{-1}	Present study
γ	Assimilation rate	0.55	%	Kofoed (1975)
Sediment				
φ	Mean bulk density of sediment	520	$\mathrm{g\,l}^{-1}$	Present study

Biogeosciences Discuss., https://doi.org/10.5194/bg-2018-325
Manuscript under review for journal Biogeosciences
Discussion started: 10 July 2018

Table A4. Mean individual weight of *P. ulvae* (mg C)

Month	J	F	M	A	M	J	J	A	S	O	N	S
Weight	0.21	0.13	0.11	0.11	0.15	0.22	0.26	0.23	0.10	0.23	0.19	0.15